



This is a repository copy of *A glucuronoxylomannan epitope exhibits serotype-specific accessibility and redistributes towards the capsule surface during Titanisation of the fungal pathogen Cryptococcus neoformans.*

White Rose Research Online URL for this paper:
<https://eprints.whiterose.ac.uk/142051/>

Version: Accepted Version

Article:

Probert, M., Zhou, X., Goodall, M. et al. (4 more authors) (2019) A glucuronoxylomannan epitope exhibits serotype-specific accessibility and redistributes towards the capsule surface during Titanisation of the fungal pathogen *Cryptococcus neoformans*. *Infection and Immunity*, 87 (4). e00731-18. ISSN 0019-9567

<https://doi.org/10.1128/IAI.00731-18>

© 2019 American Society for Microbiology. This is an author produced version of a paper subsequently published in *Infection and Immunity*. Uploaded in accordance with the publisher's self-archiving policy.

Reuse

Items deposited in White Rose Research Online are protected by copyright, with all rights reserved unless indicated otherwise. They may be downloaded and/or printed for private study, or other acts as permitted by national copyright laws. The publisher or other rights holders may allow further reproduction and re-use of the full text version. This is indicated by the licence information on the White Rose Research Online record for the item.

Takedown

If you consider content in White Rose Research Online to be in breach of UK law, please notify us by emailing eprints@whiterose.ac.uk including the URL of the record and the reason for the withdrawal request.



eprints@whiterose.ac.uk
<https://eprints.whiterose.ac.uk/>

1 **A glucuronoxylomannan epitope exhibits serotype-specific accessibility and**
2 **redistributes towards the capsule surface during Titanisation of the fungal**
3 **pathogen *Cryptococcus neoformans***

4
5 Mark Probert¹, Xin Zhou¹, Margaret Goodall², Simon A. Johnston³, Ewa Bielska¹,
6 Elizabeth R. Ballou¹, Robin C. May¹

7
8 ¹Institute of Microbiology & Infection and School of Biosciences, University of
9 Birmingham, Edgbaston, Birmingham, UK. B15 2TT

10
11 ²Institute of Immunology & Immunotherapy, University of Birmingham, Edgbaston,
12 Birmingham, UK. B15 2TT

13
14 ³Department of Infection, Immunity and Cardiovascular Disease and Bateson
15 Centre, University of Sheffield, Sheffield, UK. S10 2TN.

16
17 Correspondence to: r.c.may@bham.ac.uk. e.r.ballou@bham.ac.uk
18 +44-121-4145418 +44-121-414-5572

1
2
3
4
5
6
7
8
9
10
11
12
13
14
15
16
17
18
19
20
21
22
23
24
25
26
27
28
29
30
31
32
33
34
35
36
37
38
39
40
41
42

43 **Abstract**

44 Disseminated infections with the fungal species *Cryptococcus neoformans* or, less
45 frequently, *C. gattii*, are an important cause of mortality in immunocompromised
46 individuals. Central to the virulence of both species is an elaborate polysaccharide
47 capsule that consists predominantly of glucuronoxylomannan (GXM). Due to its
48 abundance, GXM is an ideal target for host antibodies, and several monoclonal
49 antibodies (mAbs) have previously been derived using purified GXM or whole
50 capsular preparations as antigen. In addition to their application in the diagnosis of
51 cryptococcosis, anti-GXM mAbs are invaluable tools for studying capsule structure.
52 In this study, we report the production and characterisation of a novel anti-GXM
53 mAb, Crp127, that unexpectedly reveals a role for GXM remodelling during the
54 process of fungal Titanisation. We show that Crp127 recognises a GXM epitope in
55 an *O*-acetylation dependent, but xylosylation-independent, manner. The epitope is
56 differentially expressed by the four main serotypes of *Cryptococcus neoformans* and
57 *gattii*, is heterogeneously expressed within clonal populations of *C. gattii* serotype B
58 strains and is typically confined to the central region of the enlarged capsule.
59 Uniquely, however, this epitope redistributes to the capsular surface in Titan cells, a
60 recently characterised morphotype where haploid 5 μm cells convert to highly
61 polyploid cells $>10 \mu\text{m}$ with distinct but poorly understood capsular characteristics.
62 Titans are produced in the host lung and critical for successful infection. Crp127
63 therefore advances our understanding of cryptococcal morphological change and
64 may hold significant potential as a tool to differentially identify cryptococcal strains
65 and subtypes.

66

67 **Introduction**

68 As the two main etiological agents of cryptococcosis, *Cryptococcus neoformans* and
69 *Cryptococcus gattii* are major contributors to the global health burden imposed by
70 invasive fungal infections (1). Whilst *C. neoformans* typically manifests as meningitis
71 in immunocompromised individuals, *C. gattii* infections are not associated with
72 specific immune defects and have been responsible for fatal outbreaks of pneumonia
73 (2–4). Central to the virulence of both species is an elaborate polysaccharide
74 capsule, without which *Cryptococcus* is rendered avirulent (5, 6). The composition of
75 this capsule is highly variable and differs between yeast cells and Titan cells (defined
76 as cells >10 μm in cell body diameter with increased ploidy and altered cell wall and
77 capsule) formed by *C. neoformans* within the host lung (7–9). Titan cells contribute
78 to pathogenesis by resisting phagocytosis, enhancing dissemination of yeast to the
79 central nervous system and altering host immune status (7, 9–13).

80

81 The cryptococcal capsule consists of ~90% glucuronoxylomannan (GXM), ~10%
82 glucuronoxylomannogalactan (GXMGal) and <1% mannoproteins (MPs) (14). GXM
83 is a megadalton polysaccharide containing a backbone of α -(1,3)-mannan that is
84 decorated with β -(1,2)-glucuronic acid, β -(1,2)-xylose and β -(1,4)-xylose substituents
85 (15). The backbone mannan can also be *O*-acetylated, although the position at
86 which this modification is added remains unclear for most strains (14–16). Seven
87 repeat motifs – called structure reporter groups (SRGs) – contribute to structural
88 variation in GXM (15). All SRGs contain a β -(1,2)-glucuronic acid on their first
89 mannose residue, however the number of β -(1,2)- and β -(1,4)-xylose substituents
90 varies (15). The extent and position of *O*-acetyl groups in each SRG remain unclear,
91 however xylose and *O*-acetyl groups attached to the same mannose residue appear
92 to be mutually exclusive (17). SRG usage differs between the four main serotypes of

93 *Cryptococcus*, with each strain designated a serotype based on the reactivity of its
94 capsular material with antibody preparations (18). *C. neoformans* serotypes A and D
95 tend to biosynthesise GXM containing SRGs with fewer xylose substituents than
96 those from *C. gattii* serotypes B and C (15, 19).

97

98 Whilst capsule structure differs between serotypes of *Cryptococcus*, a flexible
99 biosynthetic pathway enables rapid remodelling of the capsule under different
100 environmental conditions (20). *In vitro*, changes in *O*-acetylation have been
101 associated with cell ageing in *C. neoformans* (21), reaffirming earlier reports that
102 capsules produced within clonal populations are far from homogeneous (19, 22). *In*
103 *vivo*, changes in capsule size and structure coincide with the infection of different
104 organs and likely enhance fitness through the evasion of host immunity (23–25). In
105 light of these observations, it is perhaps unsurprising that capsules produced by
106 Titan cells are structurally distinct from those produced by typical yeast cells (7, 11,
107 26). As the increased chitin content of cell walls produced by Titan cells is
108 associated with activation of a detrimental T_H2 immune response during
109 cryptococcosis (27), it is possible that hitherto unidentified structural differences in
110 Titan cell capsules also contribute to the modulation of host immunity by this *C.*
111 *neoformans* morphotype.

112

113 Alterations in capsule structure are likely to affect how *Cryptococcus* is perceived by
114 host immune molecules, with antibodies particularly sensitive to small changes in
115 molecular structures. Following exposure to cryptococci, immunoglobulin M (IgM)
116 antibodies are the most abundant isotype of antibody produced in response to GXM
117 (28). As a repetitive capsular polysaccharide, GXM is a T-independent type 2

118 antigen and antibodies generated against it utilise a restricted set of variable region
119 gene segments (29). Using monoclonal antibodies (mAbs) in conjunction with
120 mutants harbouring specific defects in GXM modification (17, 30, 31), it has been
121 determined that *O*-acetylation and, to a lesser extent, xylosylation of GXM are
122 important for epitope recognition by anti-GXM antibodies (16, 30). Whilst there is no
123 consensus surrounding the effect of GXM *O*-acetylation on virulence (17, 32), its
124 influence on antibody binding suggests that changes in GXM *O*-acetylation could be
125 a strategy deployed by cryptococci to avoid recognition by immune effectors.
126 Additionally, despite the immunomodulatory roles for GXM *O*-acetylation that have
127 been identified (30, 33), receptors that bind *O*-acetylated GXM remain elusive (34).
128 Due to the enigmatic nature of this modification within the primary virulence factor of
129 cryptococci, further investigation of GXM *O*-acetylation will help unravel the
130 complexities of cryptococcal capsule structure with the ultimate aim of understanding
131 the strategies deployed by this fatal fungal pathogen to evade host immunity.

132

133 In the present study, we report the generation of Crp127, a murine IgM mAb, using a
134 cocktail of heat-killed *C. neoformans* H99 (serotype A) (35) heat-killed *C. gattii* R265
135 (serotype B) (36) and their lysates as an immunogen. Characterisation of Crp127
136 demonstrated that it is an *O*-acetyl-dependent anti-GXM mAb specific to an epitope
137 expressed by the four *Cryptococcus* serotypes in a serotype-specific manner. Having
138 subsequently found that this epitope is heterogeneously expressed within serotype B
139 populations and is spatially confined to distinct regions of the enlarged capsule
140 across all strains tested, we then turned our attention to its expression by Titan cells.
141 Intriguingly, we noticed that the spatial distribution of this epitope differs within the
142 capsules produced by the three *C. neoformans* morphotypes found within Titanising

143 populations. Further analysis revealed that, under conditions permissive for
144 Titanisation, cell enlargement coincides with the gradual redistribution of this epitope
145 to the capsule surface.

146

147 **Results**

148 **Crp127 recognises a capsular epitope located in GXM**

149 During hybridoma screening, Crp127 was identified as staining the outer zone of live
150 cryptococci. We first assessed whether Crp127 recognises a capsular component by
151 performing flow cytometric analysis of three GXM-deficient mutants (R265 *cap10*Δ
152 (37), KN99α *cap59*Δ (38) and B3501 *cap67*Δ (39)), a GXMGal-deficient mutant
153 (KN99α *uge1*Δ (38)) and a mutant lacking both GXM and GXMGal (KN99α
154 *cap59*Δ*uge1*Δ (38)), using an Alexa-488-conjugated anti-IgM secondary antibody to
155 label Crp127. Unlike their corresponding wild-type strains, the GXM-deficient
156 mutants were not recognised by Crp127 (fig. 1A-C; *cap10*Δ $P < 0.05$; *cap67*Δ $P <$
157 0.01 ; *cap59*Δ $P < 0.01$; *cap59*Δ*uge1*Δ $P < 0.01$, Student's t-test). In contrast, the
158 GXMGal-deficient *uge1*Δ mutant was bound at levels similar to the wild-type strain
159 (fig. 1C; $P > 0.05$). Confocal microscopy corroborated these observations, with no
160 observable binding of Crp127 to GXM-deficient mutants but clear binding of Crp127
161 to the GXMGal-deficient mutant (fig. 1D-F). Taken together, these experiments
162 demonstrated that the epitope recognised by Crp127 – hereon referred to as the
163 Crp127 epitope – is a component of GXM.

164

165 **GXM O-acetylation is required for Crp127 epitope recognition**

166 Considering the importance of O-acetylation and xylosylation to the antigenic
167 signature of GXM (30), we proceeded to investigate the effect of these modifications

168 on Crp127 epitope recognition. We firstly tested the ability of Crp127 to recognise
169 two xylose-deficient mutants (JEC155 *uxs1* Δ (serotype D) (41) and KN99 α *uxs1* Δ
170 (serotype A) (38)). No significant differences were found between either *uxs1* Δ
171 mutant and their corresponding wild-type strains (fig. 2A; JEC155 *uxs1* Δ $P > 0.05$;
172 KN99 α *uxs1* Δ $P > 0.05$), indicating that xylosylation does not impact Crp127 binding.
173 In contrast, however, antibody binding was completely abrogated in the *O*-acetyl-
174 deficient *cas1* Δ mutant (fig. 2B; $P < 0.01$), indicating that *O*-acetylation of GXM is an
175 essential prerequisite for Crp127 epitope recognition.

176

177 Having made this observation, we proceeded to test two further mutants in genes
178 implicated in GXM *O*-acetylation. KN99 α *cas3* Δ exhibits a ~70% reduction in GXM
179 *O*-acetylation, whereas KN99 α *cas31* Δ exhibits subtle differences in sugar
180 composition of GXM but no reduction in GXM *O*-acetylation (42). Binding of Crp127
181 to the *cas3* Δ mutant was slightly reduced but statistically to the wild-type strain (fig.
182 2C; $P > 0.05$). This may reflect reduced density of *O*-acetylation in GXM produced by
183 this mutant. Surprisingly, however, Crp127 completely failed to recognise the
184 *cas31* Δ mutant despite this strain retaining an *O*-acetylation profile similar to the
185 wild-type (42) (fig. 2C; $P < 0.01$). To be certain that the *O*-acetyl-defective mutants
186 tested still produced capsule, we confirmed the binding of *O*-acetyl-independent anti-
187 GXM mAb F12D2 (43, 44) to each strain (fig. 2K). Thus, *CAS1* and *CAS31*
188 contribute to the formation of an *O*-acetylation dependent Crp127 epitope.

189

190 ***Cryptococcus* serotypes differ in their level of Crp127 epitope recognition**

191 Differences in the *O*-acetylation state of GXM contributes towards serotype
192 classification and is a source of structural variation within the capsule of cells from a

193 clonal population (21, 30). Therefore, with Crp127 recognising an *O*-acetyl-
194 dependent epitope, we next checked for differences in Crp127 staining between the
195 five recognised serotypes of *Cryptococcus neoformans* and *gattii*, testing two
196 independent strains of each serotype. Flow cytometry analysis demonstrated that
197 Crp127 consistently bound most effectively to serotype D strains (B3501 and
198 JEC155) (fig. 3A-B), with all cells within these populations exhibiting high-level
199 accessibility of the Crp127 epitope (fig. 3F). We detected slightly lower binding to
200 serotype A strains (fig. 3A-B), with high-level homogeneous staining also seen in the
201 case of H99, but a proportion of unstained cells from strain KN99 α (fig. 3C).
202 Interesting, the two AD hybrid strains tested (CBS 950 (47) and ZG287 (48)) were
203 notably different in regard to Crp127 binding (fig. 3A-B), with CBS 950 exhibiting low-
204 level heterogeneous staining and ZG287 showing high-level homogeneous staining
205 (fig. 3G).

206

207 The two remaining cryptococcal serotypes, B and C, together represent *C. gattii*.
208 Serotype B strains R265 and CDCR272 (36) demonstrated significantly lower
209 epitope recognition than *C. neoformans* serotypes (fig. 3A-B) and considerable
210 heterogeneity within the population (fig. 3D). Interestingly, however, serotype C
211 strains were completely unrecognised by Crp127, with neither strain CBS 10101 (49)
212 or M27055 (50) showing detectable staining (fig. 3A, B and E). From this, we
213 conclude that there are serotype-specific differences in the availability of the Crp127
214 epitope, with epitope accessibility being related to serotype in a pattern of D > A >>
215 B >>> C.

216

217 **Crp127 exhibits serotype-specific binding patterns that are not associated with**
218 **opsonic efficacy**

219 Having identified differential levels of the Crp127 epitope between serotypes using
220 flow cytometry, we next examined their patterns of binding by immunofluorescence
221 microscopy. Indirect immunofluorescence revealed an annular binding pattern for all
222 four strains representing serotypes A and D (fig. 4A and D). In line with their
223 differences in flow cytometry, the two AD hybrid strains tested showed different
224 patterns of binding, with CBS 950 showing punctate binding and ZG287 showing a
225 mix of annular and punctate staining. Both *C. gattii* serotype B strains exhibited
226 punctate binding (fig. 4B and E) whilst, in agreement with flow cytometry, no Crp127
227 binding was detected when imaging serotype C strains CBS 10101 or M27055.
228 However, *O*-acetyl-independent mAb F12D2 bound well to these strains, suggesting
229 that the lack of Crp127 binding reflects changes in GXM *O*-acetylation rather than
230 loss of capsular material (fig. 4F).

231

232 As annular and punctate binding patterns have been associated with opsonic and
233 non-opsonic anti-GXM IgM mAbs, respectively, we tested the ability of Crp127 to
234 opsonise cells from strains KN99 α (annular) and R265 (punctate). Unlike positive
235 control treatments mAb 18B7 and pooled human serum, Crp127 did not enhance
236 phagocytosis of either strain by J774 macrophage-like cells in the presence or
237 absence of serum (fig. S2). In summary, annular binding patterns are associated
238 with the high-level binding of Crp127 to *C. neoformans* serotypes A and D strains.
239 On the other hand, punctate binding is associated with low-level binding of Crp127 to
240 serotype B strains. However, under the conditions tested in this study, neither
241 binding pattern is clearly associated with opsonic efficacy.

242

243 Crp127 epitope recognition reflects serotype differences within *C. gattii*

244 Our data above indicate that Crp127 binding accurately reflects known serotyping of
245 cryptococcal strains. However, recent genomic data indicate that *C. gattii* may in fact
246 be composed of several cryptic species (51). We therefore extended our analysis of
247 this species group by investigating a further four *C. gattii* strains, representing
248 molecular subtypes VGI-VGIII. Similar levels of Crp127 epitope recognition was seen
249 for serotype B strains R265 (VGIIa), CDCR272 (VGIIb), EJB55 (VGIIc) (52) and
250 CA1873 (VGIIIa) (53) (fig. 5A-B; $P > 0.05$), however significantly higher recognition
251 was seen for the serotype B strain DSX (VGI) (54) (fig. 5A-B; $P < 0.01$). Indirect
252 immunofluorescence corroborated these findings, with punctate binding seen for the
253 four strains presenting the epitope at low levels (fig. 5D-H) and annular binding seen
254 for strain DSX (fig. 5C). We also tested strain CA1508 (VGIIIb) (55), a *C. gattii* strain
255 that, to our knowledge, has not previously been serotyped. Both flow cytometry and
256 indirect immunofluorescence showed that Crp127 did not recognise this strain (fig.
257 5A and H), implying that it is a serotype C strain. In combination with the data
258 presented in figure 3, our finding that four out of five serotype B strains were bound
259 similarly by Crp127 suggests that availability of this epitope is fairly well conserved
260 within this serotype.

261

**262 The Crp127 epitope localises to spatially confined zones of the enlarged
263 capsule and binding elicits capsular swelling reactions**

264 Having investigated the binding of Crp127 to cells with a small capsule, we next
265 wished to investigate cells that had been grown in capsule-inducing conditions, given
266 that capsule enlargement occurs shortly after infection of the host. Interestingly, in all

267 of the strains tested we saw that the Crp127 epitope was spatially confined to distinct
268 capsular regions (fig. 6). For serotype A strains H99, KN99 (fig. 6A), and CBS 8336
269 (56) (fig. S3F) and serotype D JEC21 and B3501 (fig. 6D) strains, antibody binding
270 was detected in the central zone of the capsule. Serotype B strains differed, with
271 regions adjacent to the cell wall and on the capsule surface bound by Crp127 in the
272 case of strain R265 but only the single region proximal to the surface bound in the
273 case of CDCR272 (fig. 6B). Serotype AD strain ZG287 exhibited a similar pattern of
274 binding to R265, with Crp127 binding to both an inner and outer region of the
275 capsule, however strain CBS 950 was bound in a region adjacent to the cell wall (fig.
276 6D).

277

278 The binding of mAbs to capsular GXM alters the refractive index of the enlarged
279 capsule, resulting in capsular swelling reactions that can be visualised using DIC
280 microscopy (57). In testing the ability of Crp127 to produce a capsular swelling
281 reaction with strains KN99 α , R265, B3501 and CBS 950, we observed no discernible
282 differences in the reaction pattern produced between strains, with a highly refractive
283 outer rim and a textured inner capsule characteristic for each strain (fig. 6E-H;
284 bottom panels). Notably, however, Crp127 reaction patterns differed from those
285 elicited by 18B7, which also exhibited a highly refractive outer rim but lacked texture
286 throughout the capsule (fig. 6E-H; top right panels). Taken together, our studies of
287 Crp127 binding to capsule-induced cells demonstrate that the Crp127 epitope is
288 localised to specific capsular regions and that Crp127 binding produces capsular
289 swelling reactions that are independent of serotype.

290

291 **Spatial distribution of the Crp127 epitope differs within the capsules produced**
292 **by Titanide, yeast-like and Titan cells**

293 Following infection of the host lung, a proportion of *C. neoformans* cells differentiate
294 into Titan cells, a very large morphotype that facilitates pathogenesis and is
295 associated with poor clinical outcomes (8, 12). When grown under Titanising
296 conditions *in vitro*, *C. neoformans* forms a heterogeneous population of small, oval-
297 shaped Titanide cells (thin-walled cells 2-4 μm in diameter that are distinct from
298 thick-walled 1 μm micro-cells), yeast-like cells ($\sim 5 \mu\text{m}$) and large Titan cells ($>10 \mu\text{m}$)
299 (9, 58). As differences in capsule are known to exist between yeast and Titan cells
300 (26, 59), we tested whether Crp127 could distinguish the morphological subtypes
301 found in Titanising populations from strains H99 and KN99 α , two closely-related
302 strains for which Titanisation has been extensively studied (7, 9, 11, 26, 60). Indeed,
303 when these strains were grown under Titanising conditions *in vitro* and imaged, we
304 noticed differences in the spatial distribution of the Crp127 epitope within the
305 capsules produced by cells of different sizes (fig. 7A and fig. S3A). Cells 2-4 μm
306 were poorly recognised by Crp127 (fig. 7A), suggesting these cells did not produce
307 the epitope or that they were had budded after the immunostaining procedure.
308 Crp127 bound to a capsular region adjacent to the cell wall in smaller yeast cells,
309 within the central zone of the capsule in larger yeast-like cells and close to the
310 capsule surface of Titan cells (fig. 7A and fig. S3A). In order to quantify how cell size
311 affects capsular distribution of the Crp127 epitope, we determined the ratio between
312 the area of capsule encompassed by the Crp127 epitope and the area of the whole
313 capsule; using this metric, a ratio approaching 1 is indicative of the epitope being
314 found in close proximity to the capsule surface (fig. 7B). Across three biological
315 repeats (with a mean number of 111 and 133 cells measured for strains H99 and

316 KN99 α , respectively), mean (\pm standard error of the mean) ratios of 0.07 ± 0.02 and
317 0.05 ± 0.02 were calculated for cells 2-4 μm in diameter for strains H99 and KN99 α ,
318 respectively, consistent with our initial observations that Crp127 bound near to the
319 cell wall or not at all in the smallest cells (fig. 7C and fig. S3B). For cells 4-10 μm ,
320 mean ratios were 0.42 ± 0.03 and 0.40 ± 0.01 for strains H99 and KN99 α ,
321 respectively (fig. 7C and fig. S3B), indicating the Crp127 epitope is predominantly
322 located in the central zone of the capsule in 4-10 μm cells, as we had previously
323 observed (fig. 6A). Finally, the mean ratios for cells >10 μm in diameter were $0.72 \pm$
324 0.03 and 0.71 ± 0.03 for strains H99 and KN99 α respectively, making them
325 significantly higher than those calculated for both 2-4 μm (fig. 7C and fig. S3B; H99
326 $P < 0.001$; KN99 α $P < 0.001$) and 4-10 μm cells (fig. 7C and S3B; H99 $P < 0.001$;
327 KN99 α $P < 0.001$). In summary, our results demonstrate that Crp127 binds closer to
328 the capsule surface of Titan cells than Titanide and yeast-like cells in the widely used
329 serotype A strains H99 and KN99 α .

330

331 **Migration of the Crp127 epitope towards the surface of the capsule coincides**
332 **with cell enlargement**

333 To investigate the effect of small changes in cell size on Crp127 epitope distribution,
334 we plotted cell body diameter against epitope proximity to the capsule surface for all
335 H99 and KN99 α cells measured (fig. 7D and fig. S3C). In doing so, we identified a
336 positive correlation between cell body diameter and epitope proximity to the capsule
337 surface of yeast-like cells. In agreement with this, when plotting only cells of cell
338 body diameter 4-10 μm , we found a positive correlation between cell body diameter
339 and epitope proximity to the capsule surface in both strains tested (fig. 7E and fig.

340 S3D; H99 $r = 0.65$; KN99 α $r = 0.66$). Unlike cell body diameter, capsule diameter did
341 not correlate with epitope proximity to the capsule surface, indicating that changes in
342 capsule size do not explain changes in the proximity of the Crp127 to the capsule
343 surface (fig. 7F and fig. S3E).

344

345 Acknowledging the genetic similarities between strains H99 and KN99 α , we also
346 investigated serotype A strain CBS 8336 (56), serotype D strain B3501 and serotype
347 B strain R265. Previously, a *C. gattii* strain R265 isolate failed to Titanise *in vitro*
348 using the serum induction protocol, but was observed to form $<10 \mu\text{m}$ Titan-like cells
349 using an alternate protocol (9, 60, 61). Using a different source of R265, we were
350 able to observe limited Titans in this strain using serum induction (Figure S3F). In
351 addition, *C. neoformans* strains CBS 8336 and B3501 both formed Titan cells
352 (Figure S3F). Although Crp127 binding appeared to be redistributed outwards during
353 Titanisation of CBS 8336 and R265, redistribution was less apparent in the case of
354 B3501 (fig. S3F). Thus, the extent of epitope redistribution during Titanisation may
355 vary between strains.

356

357 Our results suggest that, in two strains frequently used for the study of Titanisation,
358 the Crp127 epitope moves gradually to the capsule surface as cells enlarge, raising
359 the question of how this may occur. Throughout our imaging experiments, the
360 binding of Crp127 to the majority of Titanide and yeast-like cells (in addition to all
361 Titan cells) produced an annular immunofluorescence binding pattern (fig. 7F; top
362 row). However, we also noticed that some Titanide and yeast-like cells produced a
363 second more faint ring of Crp127 epitope outside of this typical annular ring (fig. 7F;
364 bottom row). This may represent the addition of Crp127 epitope closer to the capsule

365 surface, partially explaining how redistribution of this epitope coincides with cell
366 enlargement.

367

368 **Discussion**

369 In this study, we demonstrated that a capsular epitope recognised by Crp127 – an
370 anti-GXM mAb produced in our laboratory – contributes to serotype-specific
371 differences in capsule structure. This epitope traverses the capsule as cells enlarge
372 under conditions permissive for Titanisation, resulting in its differential distribution
373 throughout the capsule of the three *C. neoformans* morphotypes found within
374 Titanising populations of two strains used to model cryptococcal Titanisation.
375 Detailing the accessibility and localisation of this epitope adds to the existing body of
376 literature surrounding the variability of the cryptococcal capsule between strains and
377 reveals yet another way in which Titan cell capsules are structurally distinct from
378 those produced by yeast cells (21–23, 32, 62).

379

380

381 Based on our examination of a panel of mutants harbouring capsule defects, we
382 propose that Crp127 is an anti-GXM mAb whose binding depends on GXM O-
383 acetylation, but not xylosylation. When comparing sequences of the CDRs from
384 Crp127 with four previously characterised anti-GXM IgM mAbs – namely 2D10,
385 12A1, 13F1 and 21D2 – we found that Crp127 CDRs were significantly different,
386 particularly with regard to the light-chain variable (V_L) CDRs. These differences
387 reflect differential gene usage and are likely to manifest as differences in epitope
388 specificity (46, 63). In contrast, when we aligned the heavy-chain variable (V_H) and
389 V_L sequences from Crp127 with those from anti-GXM IgG1 mAb 302, we noticed that

390 the sequences were extremely similar as a result of identical variable region gene
391 segment usage by these two mAbs. Identical gene segment usage is not entirely
392 surprising given the restricted set of antibody gene segments utilised by antibodies
393 specific to capsular polysaccharides (29), however the two mAbs were produced in
394 response to GXM derived from different serotypes of *Cryptococcus*. Whereas mAb
395 302 was generated following the immunisation of a mouse with serotype D GXM
396 (ATCC 24064) (64), we generated Crp127 through the immunisation of a mouse with
397 a cocktail containing both serotype A (H99) and serotype B (R265) GXM. Whichever
398 serotype of GXM activated the B cell from which Crp127 derives, the sequence
399 similarities between mAbs Crp127 and 302 demonstrate that nearly identical
400 antibodies can be elicited during infection by at least two different serotypes of
401 *Cryptococcus*.

402

403 Crp127 binding shows strong serotype dependence, with serotype D strains being
404 recognised most strongly, followed by serotype A strains. *C. gattii* serotype B strains
405 show lower, heterogeneous Crp127 epitope recognition and a punctate
406 immunofluorescence binding pattern, whilst serotype C strains entirely fail to bind the
407 antibody. Interestingly, the predominant SRG found in GXM produced by serotype D,
408 A, B and C contains 1, 2, 3 and 4 xylose substituents, respectively (15, 65). Together
409 with the previous observation that β -(1,2)-xylose and *O*-acetyl groups are not added
410 to the same backbone mannose residue (17, 42), this differential SRG usage may
411 explain the variable Crp127 epitope recognition in one of two ways. For example, the
412 additional xylose substituents present in the predominant SRG found in serotype B
413 and C GXM may prevent addition of *O*-acetyl groups in such a way that the Crp127
414 epitope is not formed. Alternatively, the extra xylose substituents found in these

415 SRGs may sterically hinder binding of Crp127 to its epitope. Studies that further
416 elucidate the roles of specific proteins in GXM biosynthesis – together with advances
417 in techniques that enable chemical synthesis of GXM oligosaccharides – will
418 enhance our understanding of how epitope recognition is achieved by anti-GXM
419 mAbs like Crp127. Intriguingly, a recent transcriptomics study identified *CAS31* as
420 being absent from the genome of strain CBS 10101 (66), a serotype C isolate that
421 we subsequently found was not recognised by Crp127. Whilst we cannot rule out the
422 possibility that other factors contribute to the inability of Crp127 to recognise
423 serotype C strains, it is tempting to speculate that the loss of *CAS31* function in this
424 lineage may explain its lack of reactivity with Crp127 (32, 34). The molecular basis
425 for *CAS31*-dependent epitope recognition remains to be determined, however, the
426 *cas31*Δ has been shown to harbour minor alterations in GXM xylose composition
427 (38). Therefore xylosylation may be in competition with O-acetylation at Crp127
428 target residues (17). Consistent with this, anti-GXM mAbs CRND-8, 21D2 and 13F1
429 also fail to recognise *cas31*Δ mutants (38), suggesting overall changes in capsule
430 organisation in this mutant.

431

432 Perhaps our most striking observation regarding the Crp127 epitope was its
433 differential distribution throughout the capsules produced by Titanide, yeast-like and
434 Titan cells of strains H99 and KN99α. Structural differences in Titan capsule
435 compared to yeast capsule have been demonstrated previously by SEM and staining
436 with the anti-capsule antibody 18B7 (7). Additionally, mAb 18B7 staining of *in vivo*-
437 derived Titan cells was heterogenous across individual Titans, including annular,
438 exterior and interior localisations in different cells (7). Using a hypoxic *in vitro* Titan
439 induction protocol, Hommel subsequently showed that there were no differences in

440 localisation of the anti-GXM mAbs E1, 2D10 or 13F1 in Titans compared to yeast
441 (59). Therefore, the consistent progression in localisation pattern across cell types
442 shown here appears to be a unique feature of the Crp127 epitope (7). The positive
443 correlation between cell size and Crp127 epitope proximity to the capsule surface is
444 suggestive of a scenario whereby the epitope is initially produced in a capsular
445 region adjacent to the cell wall in small Titanide cells before redistributing first to the
446 midzone of yeast-like cells and eventually to the capsule surface of Titan cells. This
447 finding raises the intriguing question of how formation and removal of the Crp127
448 epitope is so tightly spatially controlled within the capsule. One possibility is that the
449 epitope could be formed at the cell surface and then move outwards as the capsular
450 material elongates. Therefore, we speculate that since the epitope moves outwards
451 at a faster rate than the capsule expands, and since the amount of epitope that
452 initially surrounds a smaller Titanide or yeast-like cell would not be sufficient to form
453 the perimeter of capsule encasing a much larger Titan cell, we instead favour a
454 model in which the epitope is enzymatically removed and added to different regions
455 of the capsule during growth. For instance, it is possible that GXM decorated with *O*-
456 acetyl groups is added closer to the capsule surface in larger cells or that such
457 regions are “unmasked” in a different capsular region as the capsule is reshaped
458 during Titanisation (26).

459

460 To summarise, our findings demonstrate that the differential distribution of specific
461 epitopes within the cryptococcal capsule is yet another way in which Titan cells can
462 be distinguished from canonical yeast cells. We hope that this will prompt further
463 investigation into how redistribution of capsular epitopes occurs and what impact this
464 may have on *Cryptococcus* cell biology. We recently showed that Titanisation is

465 triggered by exposure to components of the bacterial cell wall (9), whilst interactions
466 between bacteria and the capsule have previously been described (67, 68). Capsule
467 also contributes to the buoyancy of *Cryptococcus* cells (69). As such, the importance
468 of redistributing capsular epitopes during Titanisation should be considered in the
469 context of *Cryptococcus* cell biology in both the environment and during infection.

470

471

472

473 **Materials and methods**

474 **Reagents, strains and mAbs**

475 All reagents were purchased from Sigma-Aldrich unless stated otherwise. The
476 *Cryptococcus* strains used in this study are described in table S1. The anti-GXM
477 mAbs used in this study are described in table S2.

478

479 **Growth of cryptococci**

480 *Cryptococcus* strains were preserved at -80°C in MicroBank™ tubes (Thermo Fisher
481 Scientific) prior to being stored on yeast extract peptone dextrose (YPD) agar plates
482 at 4°C for a maximum of 30 days. Unless stated otherwise, strains were cultured on
483 a rotary wheel at 20 rpm for 24 h at 25°C in round-bottom culture tubes containing 3
484 mL YPD broth. To induce capsule growth, *Cryptococcus* cells were grown in round-
485 bottom culture tubes containing 3 mL Dulbecco's Modified Eagle's Media (DMEM)
486 supplemented with 2 mM L-glutamine, 100 U/mL penicillin, 100 U/mL streptomycin
487 and 10% foetal bovine serum (FBS) for 72 h in an incubator at 37°C and 200 rpm.

488

489 **Hybridoma production and mAb purification**

490 Cultures of *C. neoformans* H99 and *C. gattii* R265 were microfuged (4000 x *g* for 5
491 min) and washed three times in 1 mL Dulbecco's phosphate-buffered saline (PBS).
492 Washed cultures were then heat killed for 60 minutes at 65°C. Following heat killing
493 20 µL was plated onto YPD to confirm there were no viable cells. Heat-killed H99
494 and R265 cells were then either lysed (see below) or mixed 1:1 and stored at -20°C
495 prior to inoculation. Fungal cells were lysed using Precellys tubes (UK05 03961-1-
496 004) using programme 6400-2x10-005. Following lysis, lysis beads were microfuged
497 (3000 x *g* for 1 min) and supernatant collected. H99 and R265 lysates were mixed
498 1:1 and stored at -20°C.

499

500 BALB/c mice were hyper-immunised with heat-killed H99 and R265 in addition to
501 their lysates. Hybridomas were generated by a method that has previously been
502 described (70). NS0 immortal fusion partner cells were fused with splenocytes
503 mediated by polyethylene glycol (StemCell Technologies). All animal work was
504 conducted in accordance with Home Office guidelines and following local ethical
505 approval granted under animal licence 30/2788. Supernatants from clones were
506 screened for reactivity with H99 and R265 cells using 96-well plates, with FITC-
507 conjugated anti-mouse IgG and anti-mouse IgM antibodies used to identify positive
508 clones via epifluorescence microscopy. Positive clone 127 was cultured in RPMI
509 1640 with IgG-depleted FBS and supernatant collected in a MiniPerm bioreactor
510 (Sarstedt). MAb Crp127 was purified from supernatant using affinity chromatography
511 and ProSep Thiosorb (Millipore).

512

513 **Hybridoma sequencing and antibody sequence analysis**

514 Sequencing of hybridomas was carried out by Absolute Antibody Ltd (UK).
515 Sequencing was performed by whole transcriptome shotgun sequencing (RNA-Seq).
516 In brief, hybridomas were cultured in Iscove's Modified Dulbecco's Media (IMDM)
517 supplemented with 10% FBS in an incubator at 37°C and with 5% CO₂. Total RNA
518 was extracted from cells and a barcoded cDNA library generated through RT-PCR
519 using a random hexamer. Sequencing was performed using an Illumina HiSeq
520 sequencer. Contigs were assembled and annotated for viable antibody sequences
521 (i.e those not containing stop codons) to confirm the species and isotype of mAb
522 Crp127 as murine and IgM, respectively.

523

524 Variable region gene usage was determined using VBASE2 software (71) and CDRs
525 were predicted using the Kabat numbering system (72). Heavy-chain variable (V_H)
526 and light-chain variable (V_L) sequences of mAb Crp127 were aligned with antibody
527 sequences that have previously been described (40, 73). Amino acid sequences
528 were aligned using Clustal Omega software (74) and annotated using ESript
529 software (75).

530

531 **Immunolabelling**

532 *Cryptococcus* cells were immunostained for flow cytometry and microscopy
533 experiments. 1 mL of fungal culture was transferred to a 1.5 mL microcentrifuge
534 tube, microfuged (15,000 x *g* for 1 min) and washed 3x in PBS. Cell density was
535 determined using a haemocytometer and adjusted to 10⁷ cells/mL in a final volume
536 of 200 µL. 20 µg/mL Crp127, F12D2, 18B7 or mouse anti-human IgG (IgM isotype
537 control) were added and samples mixed on a rotary wheel at 20 rpm for 1 h at room
538 temperature. Untreated cells for use in flow cytometry were left untreated. After

539 primary antibody treatment, samples were microfuged (15,000 x *g* for 1 min) and
540 washed 3x in PBS to remove unbound primary antibody. 2 µg/mL Alexa-488-
541 conjugated goat anti-mouse IgM (heavy chain) (Thermo Fisher Scientific), Alexa-
542 647-conjugated goat anti-mouse IgM µ-chain (Abcam) or Alexa-647-conjugated
543 F(ab')₂-Goat anti-Mouse IgG (H+L) (Thermo Fisher Scientific) were added to
544 antibody-treated samples and samples mixed on a rotary wheel at 20 rpm for 1 h at
545 room temperature. Secondary antibody was also added to isotype control samples
546 for flow cytometry. For microscopy experiments, 5 µg/mL calcofluor-white (CFW)
547 was also added at this stage to label chitin. Following incubation with secondary
548 antibody, samples were again microfuged (15,000 x *g* for 1 min) and washed 3x to
549 remove unbound secondary antibody and CFW.

550

551 **Flow cytometry**

552 Flow cytometry experiments were performed with an Attune NxT Flow Cytometer
553 equipped with an Attune Autosampler (Thermo Fisher Scientific). Untreated, isotype
554 control and either Crp127 or 18B7 samples were prepared for each strain or
555 conditions tested. Following immunostaining, samples were diluted to 5 x 10⁶
556 cells/mL and 200 µL of *Cryptococcus* put into individual wells of a plastic round-
557 bottom 96-well plate ready for insertion into the Attune Autosampler. Sample was
558 collected from each well at a rate of 100 µL/min until 10,000 events were recorded.
559 The 488 nm laser was used to detect primary antibody bound by Alexa-488-
560 conjugated secondary antibodies, with the same voltage used to power the laser
561 within each experiment. Flow cytometry data was then analysed using FlowJo (v10)
562 software. Debris was excluded by using the FSC-A vs. SSC-A gating strategy,
563 followed by exclusion of doublets using the FSC-A vs. FSC-H gating strategy (fig.

564 S4). Exclusion of doublets was used to avoid inclusion of cell aggregates that may
565 happen due to incomplete budding, cell-cell adhesion, or antibody-mediated
566 agglutination. Where GXM-deficient mutants were analysed, samples were only
567 gated to exclude debris due to the inseparable large aggregates formed by these
568 mutants as a result of budding defects. After gating, histograms of fluorescence
569 intensity were plotted and the median fluorescence intensity (MFI) determined.
570 Corrected MFI values were calculated by subtracting the MFI value of the mAb-
571 treated sample by the corresponding isotype control sample in the case of Crp127 or
572 untreated sample where 18B7 was used. Across all experiments, MFI values
573 returned from isotype control cells were extremely similar to those returned from
574 untreated cells.

575

576 **Confocal microscopy**

577 Following the final washes of the immunostaining procedure, 2 μ L of stained
578 cryptococcal cells were spotted onto a glass slide and placed under a square glass
579 coverslip. Where visualisation of the capsule was necessary, 2 μ L Indian ink was
580 also added to the glass slide. Imaging was performed on a Nikon A1R laser
581 scanning confocal microscope using a 100x object lens and oil immersion. Alongside
582 transmitted light, 639 nm and 405 nm lasers were used to detect Alexa-647-
583 conjugated secondary antibodies and CFW, respectively. For cells with small
584 capsules, Z-stacks spanning 8 μ m were generated using steps of 0.27 μ m. For
585 capsule-induced cells, Z-stacks were taken across 20 μ m using steps of 0.66 μ m.
586 Generation of maximum intensity projections (MIPs) and other image processing
587 was performed using NIS-Elements and ImageJ software.

588

589 **Chemical de-*O*-acetylation of capsular GXM**

590 Where chemical de-*O*-acetylation of the capsule was required, cells were grown in
591 YPD broth that had been adjusted pH 11 with NaOH and sterilised with a 0.22 μm
592 filter. Round-bottom culture tubes containing 3 mL of pH 11 YPD broth was then
593 placed on a rotary wheel turning at 20 rpm for 24 h at 25°C. This method was
594 adapted from that used in a previous study (21).

595

596 **Phagocytosis assays**

597 Phagocytosis assays were performed using the murine macrophage-like J774A.1
598 cell line (mouse BALB/cN; ATCC[®] TIB-67[™]). Cells were cultured in DMEM
599 supplemented with 2 mM L-glutamine, 100 U/mL penicillin, 100 U/mL streptomycin
600 and 10% FBS, before 1×10^5 cells were seeded onto round glass coverslips that had
601 been placed into wells of a flat-bottom 24-well plate and incubated for 24 h at 37°C
602 and 5% CO₂. Cells of strain R265 and KN99 α were opsonised with 18B7 or Crp127
603 as described for the first incubation of the immunostaining procedure. In the same
604 way, cells were opsonised with 10% AB-human serum alone or in combination with
605 Crp127. To achieve a multiplicity of infection (MOI) of 10, 10^6 R265 or KN99 α cells
606 were then resuspended in serum-free DMEM and added to each well of J774A.1
607 cells. Following the infection, each well was gently washed 3x with 1 mL of warmed
608 PBS to remove extracellular yeast. The contents of each well were then fixed with
609 4% paraformaldehyde prior to being washed a further 3x. Cover slips were then
610 extracted from their well, any residual PBS removed by briefly submersing in sterile
611 dH₂O and mounted onto glass slides with Prolong Gold Antifade Mountant (Thermo
612 Fisher Scientific). The total number of internalised yeast cells per 100 J774A.1 cells

613 (phagocytic index) was determined by microscopic examination using a Nikon
614 TE2000-U microscope with a 60x objective lens and oil immersion.

615

616 **Capsular swelling reactions**

617 Capsule-induced cells were treated with 50 $\mu\text{g}/\text{mL}$ Crp127 or 18B7 as described for
618 the immunostaining procedure. 2 μL of *Cryptococcus* cells were then dropped onto a
619 glass slide and placed under a square glass coverslip. Imaging was performed on
620 the differential interference contrast (DIC) channel of a Nikon TE2000-U microscope
621 using a 60x objective lens with oil immersion. Image processing was performed
622 using NIS-Elements and ImageJ software.

623

624 **Titan cell experiments**

625 Titan cells that exhibit all the properties of *in vivo* Titan cells were induced *in vitro*
626 using a previously described protocol (9). *C. neoformans* H99, KN99 α , CBS 8336,
627 B3501 and *C. gattii* R265 cells were cultured in glass conical flasks containing 10 mL
628 yeast nitrogen base (YNB) + 2% glucose at 30°C and 200 rpm for 24 h. Cells were
629 adjusted to an OD₆₀₀ reading of 0.001 before being transferred into 10% heat-
630 inactivated foetal calf serum (HI-FCS) at a final volume of 3 mL in a plastic six-well
631 plate and grown for 72 h at 37°C and 5% CO₂. To begin a culture derived solely from
632 Titan cells, cells were passed through an 11 μm filter, trapping only larger cells on
633 the filter paper. This filter paper was then washed in PBS to re-suspend Titan cells.
634 Between 10³ and 10⁴ Titan cells were then transferred into 3 mL HI-FCS in a plastic
635 six-well plate and cultured for a further 72 h at 37°C and 5% CO₂. Titanising
636 populations were prepared for imaging according to the method described for

637 immunostaining. Imaging was performed on a Nikon TE2000-U microscope using a
638 60x objective lens with oil immersion.

639

640 To quantify the proximity of the Crp127 epitope to the capsule surface, ImageJ
641 software was used to draw regions of interest (ROIs) around the cell body, the
642 immunofluorescence binding pattern of the Crp127 and the capsule surface (as
643 determined by Indian ink staining). For each cell measured, the area of these three
644 ROIs was determined before the area of the cell body was subtracted from the areas
645 calculated for both the Crp127 epitope ROI and the capsule surface ROI. Finally, the
646 area of the Crp127 epitope ROI was divided by the capsule surface ROI as a means
647 of quantifying the proximity of the Crp127 epitope to the capsule surface. For cells
648 where no antibody binding was detected, the ratio was scored as 0. A mean number
649 of 111 and 133 cells were measured per biological replicate for strain H99 and
650 KN99 α , respectively. Image processing was performed using NIS-Elements
651 software.

652

653 **Experimental design and statistical analysis**

654 For each experiment described, three biological repeats were performed as
655 independent experiments that were carried out on different days. All datasets were
656 analysed using GraphPad Prism 7 or 8 software.

657

658 **Acknowledgements**

659 **Provision of antibodies, strains and assistance**

660 We gratefully acknowledge our colleagues Tamara Doering (Washington University),
661 Guilhem Janbon (Institut Pasteur), Arturo Casadevall (Johns Hopkins) and Thomas

662 Kozel (University of Nevada) providing antibodies and strains and for their invaluable
663 advice regarding this project. We are also grateful to Alessandro Di Maio, Leanne
664 Taylor-Smith and Joao Correia (University of Birmingham) for assistance with
665 confocal microscopy and subsequent image processing.

666

667 **Author contributions**

668 Experiments were designed and conducted by MP, XZ and EB. The Crp127 antibody
669 was raised and initially characterised by SAJ and MG. ERB and RCM helped design
670 and oversee this project. Data figures and text were prepared by MP and then edited
671 and revised by all the other authors.

672

673 **Competing interests**

674 The authors declare no competing interests with this work.

675

676 **Funding**

677 This work was made possible via funding from the Lister Institute for Preventive
678 Medicine and the European Research Council under the European Union's Seventh
679 Framework Programme (FP/2007-2013)/ERC Grant Agreement No. 614562 and
680 from the Biotechnology and Biological Sciences Research Council (BBSRC) via
681 grant BB/R008485/1. RCM is additionally supported by a Wolfson Royal Society
682 Research Merit Award. ZX is supported by a Studentship from the Darwin Trust.
683 ERB is supported by the UK Biotechnology and Biological Research Council
684 (BB/M014525/1) and the Wellcome Trust (211241/Z/18/Z).

685

686 **Data and materials availability:** All data needed to evaluate the conclusions drawn
687 in this paper are present in the paper and/or the supplementary materials. Additional
688 data related to this paper may be requested from the authors. The Crp127 antibody
689 described here is available via Ximbio.com.

690

691 **References**

692

- 693 1. Rajasingham R, Smith RM, Park BJ, Jarvis JN, Govender NP, Chiller TM,
694 Denning DW, Loyse A, Boulware DR. 2017. Global burden of disease of HIV-
695 associated cryptococcal meningitis: an updated analysis. *Lancet Infect Dis*
696 17:873–881.
- 697 2. MacDougall L, Fyfe M, Romney M, Starr M, Galanis E. 2011. Risk Factors for
698 *Cryptococcus gattii* Infection, British Columbia, Canada. *Emerg Infect Dis*
699 17:193–199.
- 700 3. Galanis E, Macdougall L, Kidd S, Morshed M, British Columbia Cryptococcus
701 gattii Working Group the BCC gattii W. 2010. Epidemiology of *Cryptococcus*
702 gattii, British Columbia, Canada, 1999-2007. *Emerg Infect Dis* 16:251–7.
- 703 4. Harris JR, Lockhart SR, Debess E, Marsden-Haug N, Goldoft M, Wohrle R,
704 Lee S, Smelser C, Park B, Chiller T. 2011. *Cryptococcus gattii* in the United
705 States: Clinical Aspects of Infection With an Emerging Pathogen. *Clin Infect*
706 *Dis* 53:1188–1195.
- 707 5. Granger DL, Perfect JR, Durack DT. 1985. Virulence of *Cryptococcus*
708 neoformans. Regulation of capsule synthesis by carbon dioxide. *J Clin Invest*
709 76:508–16.
- 710 6. Fromtling RA, Shadomy HJ, Jacobson ES. 1982. Decreased virulence in
711 stable, acapsular mutants of *cryptococcus neoformans*. *Mycopathologia*
712 79:23–9.

- 713 7. Zaragoza O, García-Rodas R, Nosanchuk JD, Cuenca-Estrella M, Rodríguez-
714 Tudela JL, Casadevall A. 2010. Fungal Cell Gigantism during Mammalian
715 Infection. *PLoS Pathog* 6:e1000945.
- 716 8. Okagaki LH, Strain AK, Nielsen JN, Charlier C, Baltes NJ, Chrétien F, Heitman
717 J, Dromer F, Nielsen K. 2010. Cryptococcal Cell Morphology Affects Host Cell
718 Interactions and Pathogenicity. *PLoS Pathog* 6:e1000953.
- 719 9. Dambuza IM, Drake T, Chapuis A, Zhou X, Correia J, Taylor-Smith L, LeGrave
720 N, Rasmussen T, Fisher MC, Bicanic T, Harrison TS, Jaspars M, May RC,
721 Brown GD, Yucel R, MacCallum DM, Ballou ER. 2018. The *Cryptococcus*
722 *neoformans* Titan cell is an inducible and regulated morphotype underlying
723 pathogenesis. *PLOS Pathog* 14:e1006978.
- 724 10. Okagaki LH, Nielsen K. 2012. Titan cells confer protection from phagocytosis
725 in *Cryptococcus neoformans* infections. *Eukaryot Cell* 11:820–6.
- 726 11. Crabtree JN, Okagaki LH, Wiesner DL, Strain AK, Nielsen JN, Nielsen K.
727 2012. Titan cell production enhances the virulence of *Cryptococcus*
728 *neoformans*. *Infect Immun* 80:3776–85.
- 729 12. Carter DA, Fernandes KE, Brockway A, Haverkamp M, Cuomo CA, Ogtrop F
730 Van, Perfect JR. 2018. Phenotypic variability correlates with clinical outcome in
731 *Cryptococcus* isolates obtained from Botswanan HIV/AIDS patients. *bioRxiv*
732 418897.
- 733 13. Zhou X, Ballou ER. 2018. The *Cryptococcus neoformans* Titan Cell: From In
734 Vivo Phenomenon to In Vitro Model. *Curr Clin Microbiol Reports* 1–9.
- 735 14. Casadevall A, Coelho C, Cordero RJB, Dragotakes Q, Jung E, Vij R, Wear
736 MP. 2018. The Capsule of *Cryptococcus neoformans*.
737 <https://doi.org/10.1080/2150559420181431087>.

- 738 15. Cherniak R, Valafar H, Morris LC, Valafar F. 1998. *Cryptococcus neoformans*
739 chemotyping by quantitative analysis of ¹H nuclear magnetic resonance
740 spectra of glucuronoxylomannans with a computer-simulated artificial neural
741 network. *Clin Diagn Lab Immunol* 5:146–59.
- 742 16. Cherniak R, Reiss E, Slodki ME, Plattner RD, Blumer SO. 1980. Structure and
743 antigenic activity of the capsular polysaccharide of *Cryptococcus neoformans*
744 serotype A. *Mol Immunol* 17:1025–1032.
- 745 17. Janbon G, Himmelreich U, Moyrand F, Improvisi L, Dromer F. 2001. Cas1p is
746 a membrane protein necessary for the O-acetylation of the *Cryptococcus*
747 *neoformans* capsular polysaccharide. *Mol Microbiol* 42:453–67.
- 748 18. Dromer F, Gueho E, Ronin O, Dupont B. 1993. Serotyping of *Cryptococcus*
749 *neoformans* by using a monoclonal antibody specific for capsular
750 polysaccharide. *J Clin Microbiol* 31:359–63.
- 751 19. McFadden DC, Fries BC, Wang F, Casadevall A. 2007. Capsule Structural
752 Heterogeneity and Antigenic Variation in *Cryptococcus neoformans*. *Eukaryot*
753 *Cell* 6:1464–1473.
- 754 20. McFadden D, Zaragoza O, Casadevall A. 2006. The capsular dynamics of
755 *Cryptococcus neoformans*. *Trends Microbiol* 14:497–505.
- 756 21. Gates-Hollingsworth MA, Kozel TR. 2009. Phenotypic heterogeneity in
757 expression of epitopes in the *Cryptococcus neoformans* capsule. *Mol Microbiol*
758 74:126–138.
- 759 22. Franzot SP, Mukherjee J, Cherniak R, Chen LC, Hamdan JS, Casadevall A.
760 1998. Microevolution of a standard strain of *Cryptococcus neoformans*
761 resulting in differences in virulence and other phenotypes. *Infect Immun*
762 66:89–97.

- 763 23. Rivera J, Feldmesser M, Cammer M, Casadevall A. 1998. Organ-dependent
764 variation of capsule thickness in *Cryptococcus neoformans* during
765 experimental murine infection. *Infect Immun* 66:5027–30.
- 766 24. Charlier C, Chrétien F, Baudrimont M, Mordelet E, Lortholary O, Dromer F.
767 2005. Capsule structure changes associated with *Cryptococcus neoformans*
768 crossing of the blood-brain barrier. *Am J Pathol* 166:421–32.
- 769 25. Garcia-Hermoso D, Dromer F, Janbon G. 2004. *Cryptococcus neoformans*
770 Capsule Structure Evolution In Vitro and during Murine Infection. *Infect Immun*
771 72:3359–3365.
- 772 26. Mukaremera L, Lee KK, Wagener J, Wiesner DL, Gow NAR, Nielsen K. 2018.
773 Titan cell production in *Cryptococcus neoformans* reshapes the cell wall and
774 capsule composition during infection. *Cell Surf* 1:15–24.
- 775 27. Wiesner DL, Specht CA, Lee CK, Smith KD, Mukaremera L, Lee ST, Lee CG,
776 Elias JA, Nielsen JN, Boulware DR, Bohjanen PR, Jenkins MK, Levitz SM,
777 Nielsen K. 2015. Chitin recognition via chitotriosidase promotes pathologic
778 type-2 helper T cell responses to cryptococcal infection. *PLoS Pathog*
779 11:e1004701.
- 780 28. Houpt DC, Pfrommer GS, Young BJ, Larson TA, Kozel TR. 1994.
781 Occurrences, immunoglobulin classes, and biological activities of antibodies in
782 normal human serum that are reactive with *Cryptococcus neoformans*
783 glucuronoxylomannan. *Infect Immun* 62:2857–64.
- 784 29. Rohatgi S, Pirofski L-A. 2015. Host immunity to *Cryptococcus neoformans*.
785 *Future Microbiol* 10:565–81.
- 786 30. Kozel TR, Levitz SM, Dromer F, Gates MA, Thorkildson P, Janbon G. 2003.
787 Antigenic and biological characteristics of mutant strains of *Cryptococcus*

- 788 neoformans lacking capsular O acetylation or xylosyl side chains. *Infect Immun*
789 71:2868–75.
- 790 31. Moyrand F, Klaproth B, Himmelreich U, Dromer F, Janbon G. 2002. Isolation
791 and characterization of capsule structure mutant strains of *Cryptococcus*
792 neoformans. *Mol Microbiol* 45:837–849.
- 793 32. Cleare W, Cherniak R, Casadevall A. 1999. In vitro and in vivo stability a
794 *Cryptococcus neoformans* glucuronoxylomannan epitope that elicits protective
795 antibodies. *Infect Immun* 67:3096–3107.
- 796 33. Ellerbroek PM, Lefeber DJ, van Veghel R, Scharringa J, Brouwer E, Gerwig
797 GJ, Janbon G, Hoepelman AIM, Coenjaerts FEJ. 2004. O-acetylation of
798 cryptococcal capsular glucuronoxylomannan is essential for interference with
799 neutrophil migration. *J Immunol* 173:7513–20.
- 800 34. Urai M, Kaneko Y, Ueno K, Okubo Y, Aizawa T, Fukazawa H, Sugita T, Ohno
801 H, Shibuya K, Kinjo Y, Miyazaki Y. 2015. Evasion of Innate Immune
802 Responses by the Highly Virulent *Cryptococcus gattii* by Altering Capsule
803 Glucuronoxylomannan Structure. *Front Cell Infect Microbiol* 5:101.
- 804 35. Perfect JR, Lang SD, Durack DT. 1980. Chronic cryptococcal meningitis: a
805 new experimental model in rabbits. *Am J Pathol* 101:177–94.
- 806 36. Kidd SE, Hagen F, Tscharke RL, Huynh M, Bartlett KH, Fyfe M, MacDougall L,
807 Boekhout T, Kwon-Chung KJ, Meyer W. 2004. A rare genotype of
808 *Cryptococcus gattii* caused the cryptococcosis outbreak on Vancouver Island
809 (British Columbia, Canada). *Proc Natl Acad Sci* 101:17258–17263.
- 810 37. Hu G, Kronstad JW. 2006. Gene disruption in *Cryptococcus neoformans* and
811 *Cryptococcus gattii* by in vitro transposition. *Curr Genet* 49:341–350.
- 812 38. Moyrand F, Fontaine T, Janbon G. 2007. Systematic capsule gene disruption

- 813 reveals the central role of galactose metabolism on *Cryptococcus neoformans*
814 virulence. *Mol Microbiol* 64:771–781.
- 815 39. Jacobson ES, Ayers DJ. 1979. Auxotrophic mutants of *Cryptococcus*
816 *neoformans*. *J Bacteriol* 139:318–9.
- 817 40. Casadevall A, DeShaw M, Fan M, Dromer F, Kozel TR, Pirofski LA. 1994.
818 Molecular and idiotypic analysis of antibodies to *Cryptococcus neoformans*
819 glucuronoxylomannan. *Infect Immun* 62:3864–72.
- 820 41. Moyrand F, Klaproth B, Himmelreich U, Dromer F, Janbon G. 2002. Isolation
821 and characterization of capsule structure mutant strains of *Cryptococcus*
822 *neoformans*. *Mol Microbiol* 45:837–49.
- 823 42. Moyrand F, Chang YC, Himmelreich U, Kwon-Chung KJ, Janbon G. 2004.
824 Cas3p belongs to a seven-member family of capsule structure designer
825 proteins. *Eukaryot Cell* 3:1513–24.
- 826 43. Percival A, Thorkildson P, Kozel TR. 2011. Monoclonal antibodies specific for
827 immunorecessive epitopes of glucuronoxylomannan, the major capsular
828 polysaccharide of *Cryptococcus neoformans*, reduce serotype bias in an
829 immunoassay for cryptococcal antigen. *Clin Vaccine Immunol* 18:1292–6.
- 830 44. Brandt S, Thorkildson P, Kozel TR. 2003. Monoclonal antibodies reactive with
831 immunorecessive epitopes of glucuronoxylomannan, the major capsular
832 polysaccharide of *Cryptococcus neoformans*. *Clin Diagn Lab Immunol* 10:903–
833 9.
- 834 45. Casadevall A, Cleare W, Feldmesser M, Glatman-Freedman A, Goldman DL,
835 Kozel TR, Lendvai N, Mukherjee J, Pirofski LA, Rivera J, Rosas AL, Scharff
836 MD, Valadon P, Westin K, Zhong Z. 1998. Characterization of a murine
837 monoclonal antibody to *Cryptococcus neoformans* polysaccharide that is a

- 838 candidate for human therapeutic studies. *Antimicrob Agents Chemother*
839 42:1437–46.
- 840 46. Casadevall A, Mukherjee J, Devi SJ, Schneerson R, Robbins JB, Scharff MD.
841 1992. Antibodies elicited by a *Cryptococcus neoformans*-tetanus toxoid
842 conjugate vaccine have the same specificity as those elicited in infection. *J*
843 *Infect Dis* 165:1086–93.
- 844 47. Boekhout T, Van Belkum A, Leenders ACAP, Verbrugh HA, Mukamurangwa
845 P, Swinne D, Scheffers WA. 1997. Molecular Typing of *Cryptococcus*
846 *neoformans*: Taxonomic and Epidemiological Aspects. *Int J Syst Bacteriol*
847 47:432–442.
- 848 48. Lengeler KB, Cox GM, Heitman J. 2001. Serotype AD strains of *Cryptococcus*
849 *neoformans* are diploid or aneuploid and are heterozygous at the mating-type
850 locus. *Infect Immun* 69:115–22.
- 851 49. Meyer W, Castañeda A, Jackson S, Huynh M, Castañeda E, IberoAmerican
852 Cryptococcal Study Group the ICS. 2003. Molecular typing of IberoAmerican
853 *Cryptococcus neoformans* isolates. *Emerg Infect Dis* 9:189–95.
- 854 50. Latouche GN, Huynh M, Sorrell TC, Meyer W. 2003. PCR-restriction fragment
855 length polymorphism analysis of the phospholipase B (PLB1) gene for
856 subtyping of *Cryptococcus neoformans* isolates. *Appl Environ Microbiol*
857 69:2080–6.
- 858 51. Hagen F, Khayhan K, Theelen B, Kolecka A, Polacheck I, Sionov E, Falk R,
859 Parnmen S, Lumbsch HT, Boekhout T. 2015. Recognition of seven species in
860 the *Cryptococcus gattii*/*Cryptococcus neoformans* species complex. *Fungal*
861 *Genet Biol* 78:16–48.
- 862 52. Byrnes EJ, Li W, Lewit Y, Ma H, Voelz K, Ren P, Carter DA, Chaturvedi V,

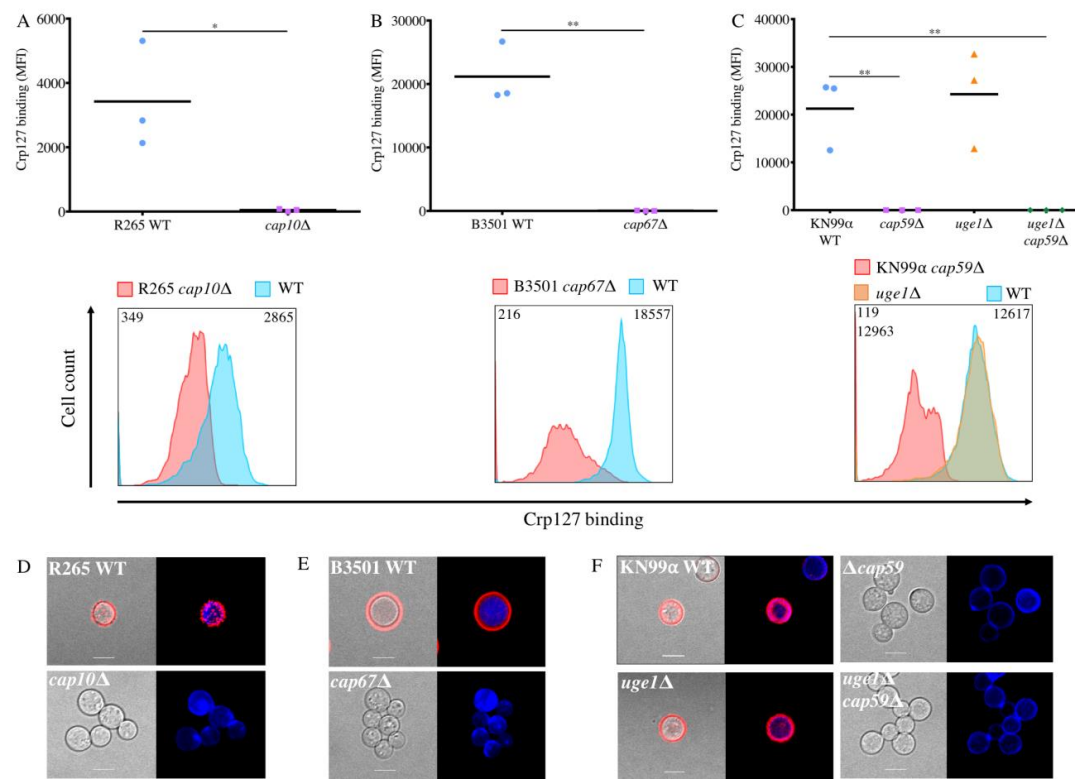
- 863 Bildfell RJ, May RC, Heitman J, Heitman J. 2010. Emergence and
864 pathogenicity of highly virulent *Cryptococcus gattii* genotypes in the northwest
865 United States. *PLoS Pathog* 6:e1000850.
- 866 53. Farrer RA, Desjardins CA, Sakthikumar S, Gujja S, Saif S, Zeng Q, Chen Y,
867 Voelz K, Heitman J, May RC, Fisher MC, Cuomo CA. 2015. Genome Evolution
868 and Innovation across the Four Major Lineages of *Cryptococcus gattii*. *MBio*
869 6:e00868-15.
- 870 54. Springer DJ, Billmyre RB, Filler EE, Voelz K, Pursall R, Mieczkowski PA,
871 Larsen RA, Dietrich FS, May RC, Filler SG, Heitman J. 2014. *Cryptococcus*
872 *gattii* VGIII isolates causing infections in HIV/AIDS patients in Southern
873 California: identification of the local environmental source as arboreal. *PLoS*
874 *Pathog* 10:e1004285.
- 875 55. Byrnes EJ, Li W, Ren P, Lewit Y, Voelz K, Fraser JA, Dietrich FS, May RC,
876 Chatuverdi S, Chatuverdi V, Heitman J. 2011. A Diverse Population of
877 *Cryptococcus gattii* Molecular Type VGIII in Southern Californian HIV/AIDS
878 Patients. *PLoS Pathog* 7:e1002205.
- 879 56. Dromer F, Fell JW, Hop WCJ, Theelen B, Diaz M, Meyer W, Abeln ECA,
880 Boekhout T. 2001. Hybrid genotypes in the pathogenic yeast *Cryptococcus*
881 *neoformans*. *Microbiology* 147:891–907.
- 882 57. Mukherjee J, Cleare W, Casadevall A. 1995. Monoclonal antibody mediated
883 capsular reactions (Quellung) in *Cryptococcus neoformans*. *J Immunol*
884 *Methods* 184:139–43.
- 885 58. Kress Y, Feldmesser M, Casadevall A. 2001. Dynamic changes in the
886 morphology of *Cryptococcus neoformans* during murine pulmonary infection.
887 *Microbiology* 147:2355–2365.

- 888 59. Hommel B, Mukaremera L, Cordero RJB, Coelho C, Desjardins CA, Sturny-
889 Leclère A, Janbon G, Perfect JR, Fraser JA, Casadevall A, Cuomo CA,
890 Dromer F, Nielsen K, Alanio A. 2018. Titan cells formation in *Cryptococcus*
891 *neoformans* is finely tuned by environmental conditions and modulated by
892 positive and negative genetic regulators. *PLOS Pathog* 14:e1006982.
- 893 60. Trevijano-Contador N, de Oliveira HC, García-Rodas R, Rossi SA, Llorente I,
894 Zaballos Á, Janbon G, Ariño J, Zaragoza Ó. 2018. *Cryptococcus neoformans*
895 can form titan-like cells in vitro in response to multiple signals. *PLOS Pathog*
896 14:e1007007.
- 897 61. Zhou X, Ballou ER. 2018. The *Cryptococcus neoformans* Titan Cell: From In
898 Vivo Phenomenon to In Vitro Model. *Curr Clin Microbiol Reports* 5:252–260.
- 899 62. Fries BC, Taborda CP, Serfass E, Casadevall A. 2001. Phenotypic switching
900 of *Cryptococcus neoformans* occurs in vivo and influences the outcome of
901 infection. *J Clin Invest* 108:1639–48.
- 902 63. Mukherjee J, Scharff MD, Casadevall A. 1992. Protective murine monoclonal
903 antibodies to *Cryptococcus neoformans*. *Infect Immun* 60:4534–41.
- 904 64. Eckert TF, Kozel TR. 1987. Production and characterization of monoclonal
905 antibodies specific for *Cryptococcus neoformans* capsular polysaccharide.
906 *Infect Immun* 55:1895–9.
- 907 65. Janbon G. 2004. *Cryptococcus neoformans* capsule biosynthesis and
908 regulation. *FEMS Yeast Res* 4:765–771.
- 909 66. Farrer RA, Ford CB, Rhodes J, Delorey T, May RC, Fisher M, Cloutman-Green
910 E, Balloux F, Cuomo CA. 2018. Transcriptional heterogeneity of *Cryptococcus*
911 *gattii* VGII compared with non-VGII lineages underpins key pathogenicity
912 pathways. *bioRxiv* 396796.

- 913 67. Abdulkareem AF, Lee HH, Ahmadi M, Martinez LR. 2015. Fungal serotype-
914 specific differences in bacterial-yeast interactions. *Virulence* 6:652–657.
- 915 68. Saito F, Ikeda R. 2005. Killing of *Cryptococcus neoformans* by *Staphylococcus*
916 *aureus*: the role of cryptococcal capsular polysaccharide in the fungal-bacteria
917 interaction. *Med Mycol* 43:603–612.
- 918 69. Vij R, Cordero RJB, Casadevall A. 2018. The Buoyancy of *Cryptococcus*
919 *neoformans* Is Affected by Capsule Size. *mSphere* 3:e00534-18.
- 920 70. Galfrè G, Milstein C. 1981. [1] Preparation of monoclonal antibodies:
921 Strategies and procedures. *Methods Enzymol* 73:3–46.
- 922 71. Retter I, Althaus HH, Münch R, Müller W. 2004. VBASE2, an integrative V
923 gene database. *Nucleic Acids Res* 33:D671–D674.
- 924 72. Wu TT, Kabat EA. 1970. An analysis of the sequences of the variable regions
925 of Bence Jones proteins and myeloma light chains and their implications for
926 antibody complementarity. *J Exp Med* 132:211–50.
- 927 73. Nakouzi A, Valadon P, Nosanchuk J, Green N, Casadevall A. 2001. Molecular
928 basis for immunoglobulin M specificity to epitopes in *Cryptococcus neoformans*
929 polysaccharide that elicit protective and nonprotective antibodies. *Infect Immun*
930 69:3398–409.
- 931 74. McWilliam H, Li W, Uludag M, Squizzato S, Park YM, Buso N, Cowley AP,
932 Lopez R. 2013. Analysis Tool Web Services from the EMBL-EBI. *Nucleic Acids*
933 *Res* 41:W597–W600.
- 934 75. Robert X, Gouet P. 2014. Deciphering key features in protein structures with
935 the new ENDscript server. *Nucleic Acids Res* 42:W320–W324.
- 936
- 937

938
939
940
941
942
943

944
945
946
947
948
949
950
951



952

953

954

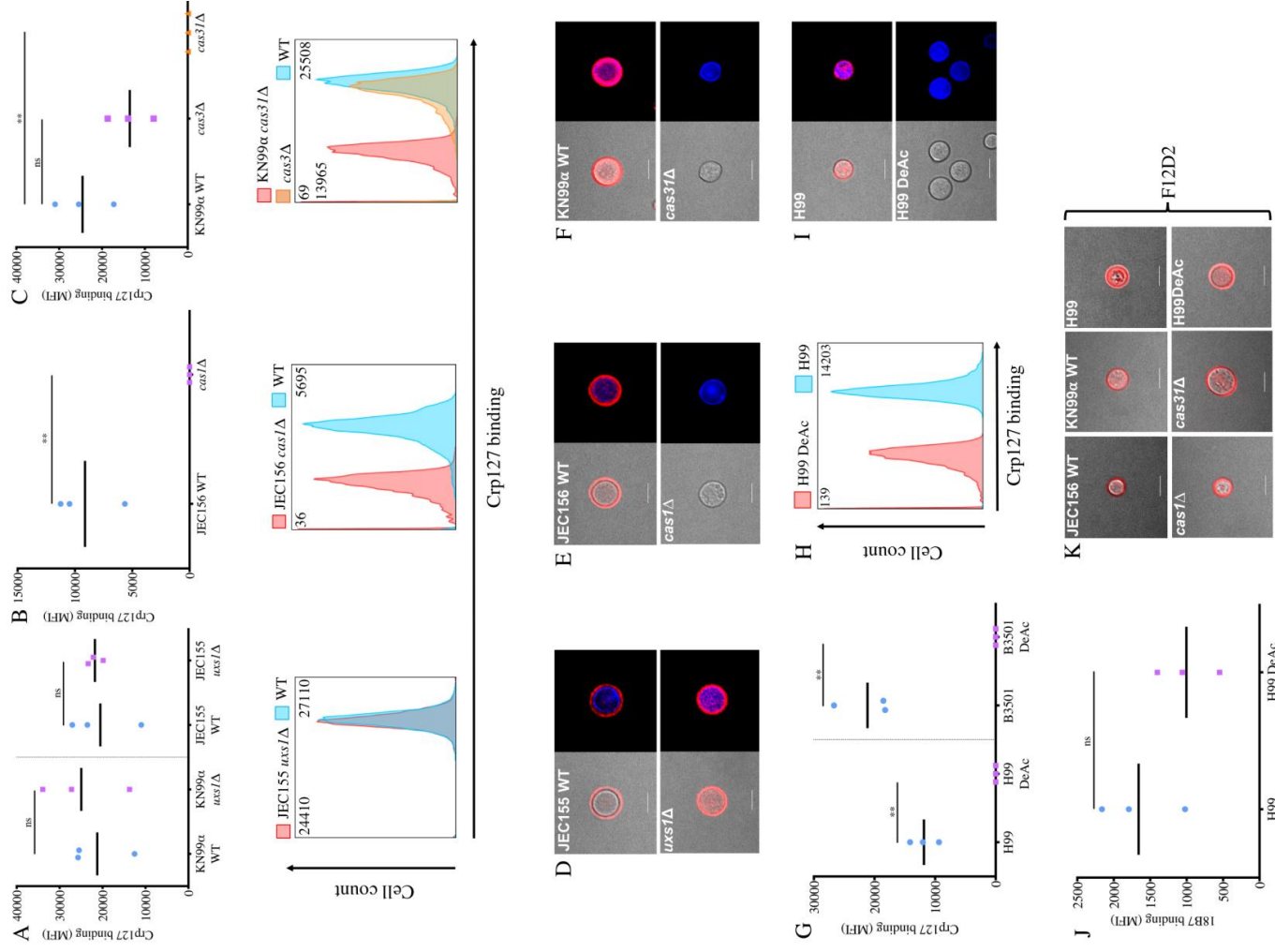
955

956 **Fig. 1. Crp127 is an anti-GXM mAb.** The ability of Crp127 to bind to GXM- and
957 GXMGal-deficient mutants of *C. gattii* and *C. neoformans* was quantified via flow
958 cytometry. Scatter plots (top row) and representative histograms (bottom row) are
959 presented for **A)** R265 cap10 Δ , **B)** B3501 cap67 Δ , **C)** KN99 α cap59 Δ , KN99 α
960 uge1 Δ , KN99 α cap59 Δ uge1 Δ and their corresponding wild-type strains. For scatter
961 plots, corrected median fluorescence intensity (MFI) values were calculated by
962 subtracting the MFI value of isotype control cells from the MFI value of the Crp127-
963 treated cells, with data points representing MFI values calculated from three
964 biological replicates performed as independent experiments. A Student's t-test was
965 used to test for statistically significant differences between R265 cap10 Δ and B3501
966 cap67 Δ and their corresponding wild-type strains, whilst one-way ANOVA followed
967 by Dunnett's multiple comparison test was used to test for statistically significant
968 differences between KN99 α cap59 Δ , KN99 α uge1 Δ cap59 Δ , KN99 α uge1 Δ and the
969 wild-type strain KN99 α ($n=3$) ($ns P > 0.05$; * $P < 0.05$; ** $P < 0.01$). Histograms show
970 a representative distribution of Crp127 binding for one or all of the strains in the
971 above scatter plot, with the colour-coded key provided for reference. Numerical
972 values in the top left and right of each histogram correspond to the MFI value
973 calculated from the strain labelled directly above. **D)** R265 cap10 Δ , **E)** B3501
974 cap67 Δ , **F)** KN99 α cap59 Δ , uge1 Δ , uge1 Δ cap59 Δ and their wild-type strains were
975 labelled for chitin using calcofluor-white (CFW; blue) and Crp127 (far-red; goat
976 Alexa-647-conjugated anti-mouse IgM μ -chain) and maximum-intensity projections

977 *generated from confocal microscopy z-stacks. Presented are representative images*
978 *merged for transmitted light and Crp127 (left panels) and Crp127 and chitin (right*
979 *panels). Scale bars represent 5 μ m.*

980

981



982

983

984

985 **Fig. 2. Crp127 requires O-acetylation, but not xylosylation, of GXM for epitope**
986 **recognition.** The ability of Crp127 to recognise mutants with specific defects in GXM
987 modification was quantified via flow cytometry. Scatter plots (top row) and
988 representative histograms (bottom row) are presented for **A)** KN99 α *uxs1* Δ , JEC155
989 *uxs1* Δ and corresponding wild-type strains; **B)** JEC156 *cas1* Δ and JEC155 wild-type
990 and **C)** KN99 α *cas3* Δ , KN99 α *cas31* Δ and KN99 α wild-type. **D)** JEC155 *uxs1* Δ , **E)**
991 JEC156 *cas1* Δ , **F)** KN99 α *cas31* Δ and corresponding wild-type strains were labelled
992 for chitin and Crp127 imaged via confocal microscopy. **G)** Binding of Crp127 to
993 chemically deacetylated cells of H99 and B3501 was quantified via flow cytometry
994 with **H)** a representative histogram presented for H99. **I)** Untreated (top) and
995 chemically deacetylated (bottom) H99 cells were labelled for chitin and Crp127 and
996 imaged via confocal microscopy. **J)** Binding of 18B7 to chemically deacetylated cells
997 of H99 and B3501 was quantified via flow cytometry. **K)** Representative cells from
998 the above strains labelled for chitin (blue) and O-acetyl-independent mAb F12D2
999 (far-red). For scatter plots, corrected MFI values were calculated by subtracting the
1000 MFI value of isotype control cells from the MFI value of the Crp127- or 18B7-treated
1001 cells, with data points representing MFI values calculated from three biological
1002 replicates performed as independent experiments. A Student's *t*-test was used to
1003 test for statistically significant differences between KN99 α *uxs1* Δ , JEC155 *uxs1* Δ
1004 and JEC156 *cas1* Δ and their corresponding wild-type strain, as well as between
1005 untreated and chemically deacetylated cells of the same strain (*n*=3). Dunnet's
1006 multiple comparison test was used to test for statistically significant differences
1007 between KN99 α Δ *cas3*, KN99 α Δ *cas31* mutants and the KN99 α wild-type strain
1008 (*n*=3) (*ns* *P* > 0.05; * *P* < 0.05; ** *P* < 0.01). Histograms show a representative
1009 distribution of Crp127 or 18B7 binding for one or all of the strains in the above

1010 scatter plot, with a colour-coded key provided for reference. Numerical values in the
1011 top left and right of each histogram correspond to the MFI value calculated from the
1012 strain labelled directly above. Representative maximum intensity projections were
1013 merged for transmitted light and Crp127 (far-red), and Crp127 and chitin (blue) (right
1014 panels). Scale bars represent 5 μm .

1015

1016

1017

1018

1019

1020

1021

1022

1023

1024

1025

1026

1027

1028

1029

1030

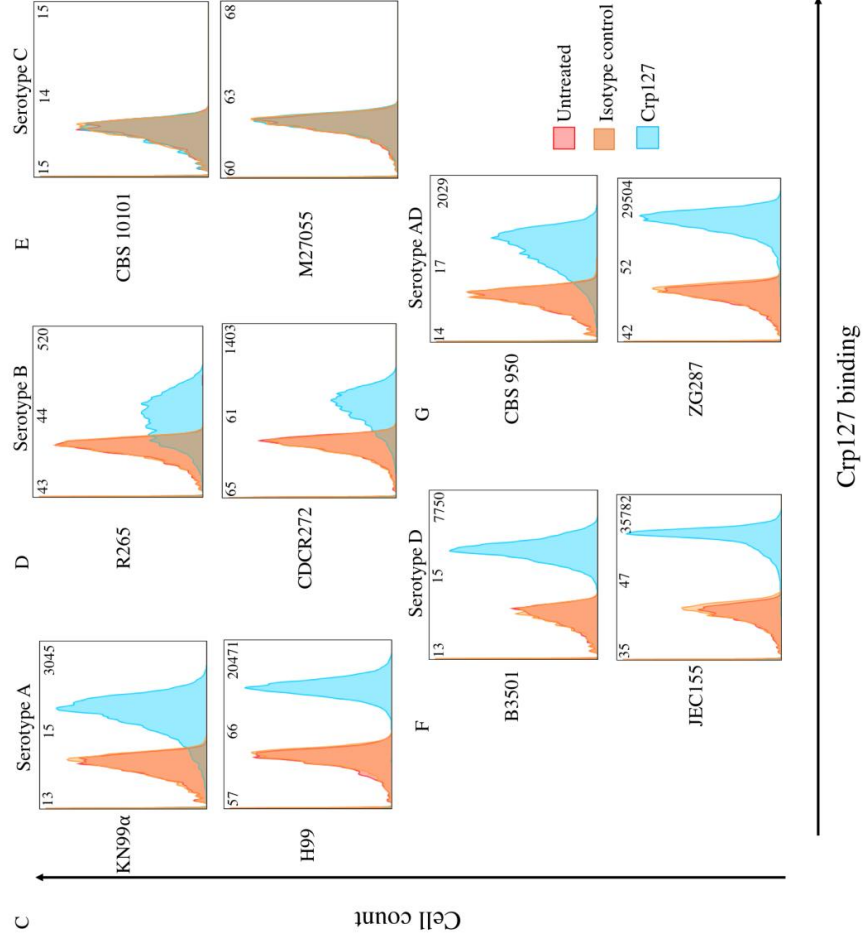
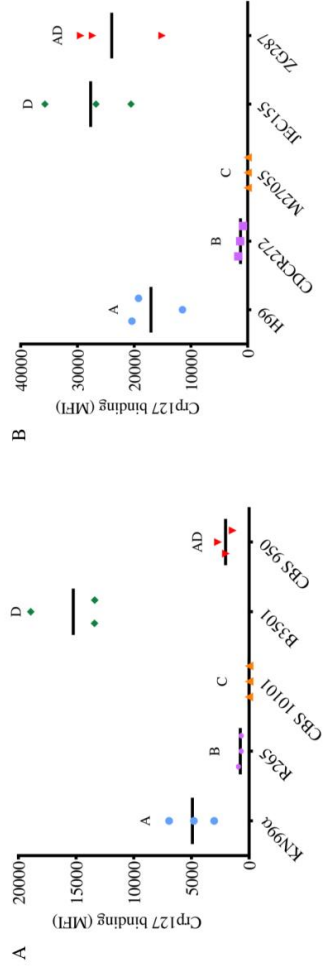
1031

1032

1033

1034

1035



1036

1037

1038

1039

1040

1041

1042 **Fig. 3. Recognition levels of the Crp127 epitope are associated with serotype.**

1043 *The ability of Crp127 to bind to two different strains from each Cryptococcus*
1044 *serotypes A, B, C, D and AD was quantified using flow cytometry. **A-B)** Scatter plots*
1045 *show corrected MFI values for each strain, which were calculated by subtracting the*
1046 *MFI value of isotype control cells from the MFI value of the corresponding Crp127-*
1047 *treated cells. Data points represent MFI values calculated from three biological*
1048 *replicates performed as independent experiments (n=3). Histograms show a*
1049 *representative distribution of Crp127 binding for **C)** serotype A strains KN99 α and*
1050 *H99, **D)** serotype B strains R265 and CDCR272, **E)** serotype C strains CBS 10101*
1051 *and M27055, **F)** serotype D strains B3501 and JEC155 and **G)** serotype AD hybrid*
1052 *strains CBS 950 and ZG287. Fluorescence intensity values for untreated, isotype*
1053 *control and Crp127-treated cells are presented in red, blue and orange, respectively,*
1054 *with corresponding MFI values displayed in the top left, centre and right of each*
1055 *panel.*

1056

1057

1058

1059

1060

1061

1062

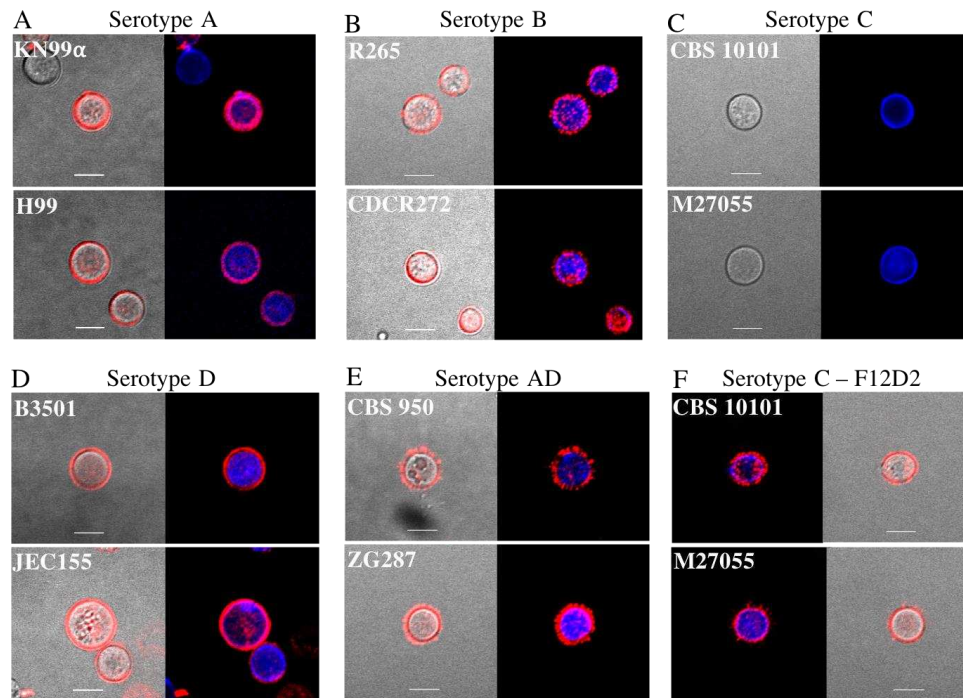
1063

1064

1065

1066

1067



1068

1069

1070

1071

1072

1073

1074

1075

1076

1077

1078

1079

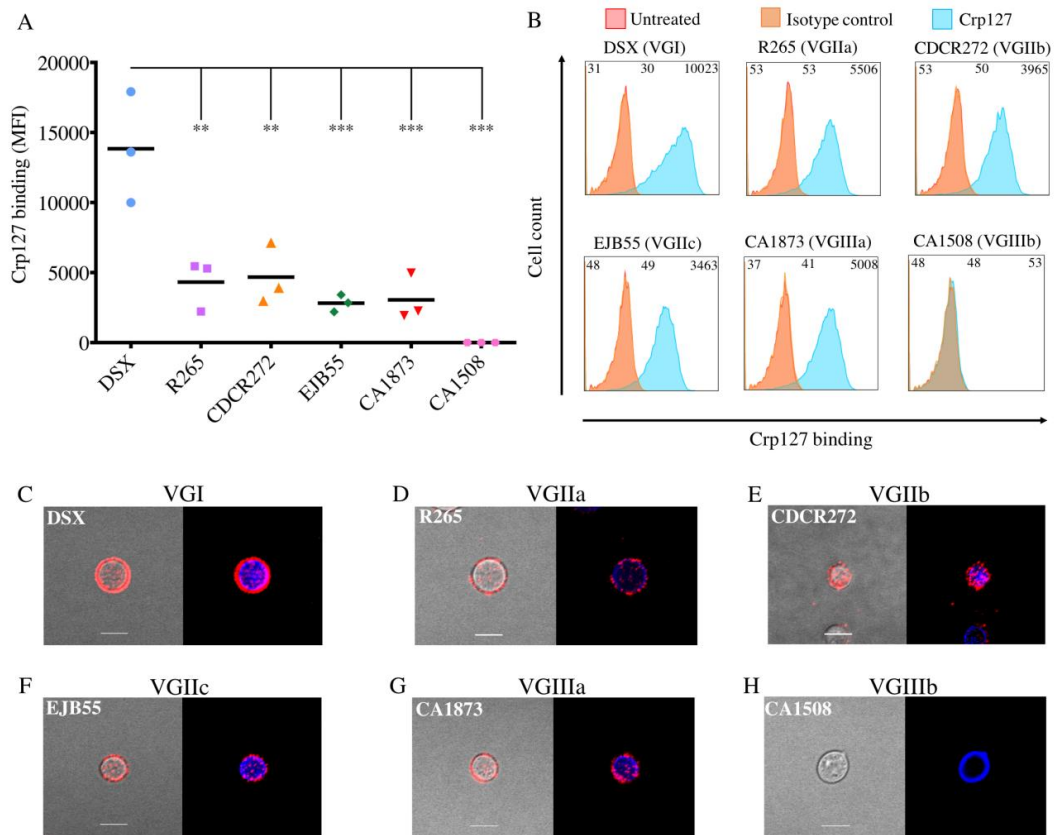
1080

1081

1082 **Fig. 4. The immunofluorescence-binding pattern of Crp127 correlates with**
1083 **serotype.** Two *Cryptococcus* strains from **A)** serotype A (KN99 and H99), **B)**
1084 serotype B (R265 and CDCR272), **C)** serotype C (CBS 10101 and M27055), **D)**
1085 serotype D (B3501 and JEC155) and **E)** serotype AD (CBS 950 and ZG287) were
1086 labelled for chitin (blue; CFW) and Crp127 (far-red; goat Alexa-647-conjugated anti-
1087 mouse IgM μ -chain). **F)** Representative cells from serotype C strains CBS 10101
1088 and M27055 labelled for chitin (blue) and O-acetyl-independent mAb F12D2 (far-red;
1089 Alexa-647-conjugated F(ab')₂ goat anti-Mouse IgG (H+L)). Maximum-intensity
1090 projections were generated via confocal microscopy. Representative images are
1091 shown for each strain. Images are merged for transmitted light and Crp127 (left
1092 panels) and Crp127 and chitin (right panels). Scale bars represent 5 μ m.

1093
1094
1095
1096
1097
1098
1099
1100
1101
1102
1103
1104
1105
1106

1107
 1108
 1109
 1110
 1111
 1112
 1113
 1114
 1115
 1116
 1117
 1118
 1119



1120 **Fig. 5. Recognition of the Crp127 epitope is largely consistent within *C. gattii***
1121 **serotypes.** The ability of Crp127 to bind to six strains from *C. gattii* that encompass
1122 molecular types VGI-VGIIIb was quantified via flow cytometry. **A)** Scatter plots show
1123 corrected MFI values for each strain, which were calculated by subtracting the MFI
1124 value of isotype control cells from the MFI value of the corresponding Crp127-treated
1125 cells. Data points represent MFI values calculated from three biological replicates
1126 performed as independent experiments. Tukey's multiple comparisons test was used
1127 to test the statistical significance of differences between the six strains ($n=3$) (ns $P >$
1128 0.05 ; $**$ $P < 0.01$; $***$ $P < 0.001$). **B)** Histograms show a representative distribution of
1129 Crp127 binding for strains DSX (VGI), R265 (VGIIa), CDCR272 (VGIIb), EJB55
1130 (VGIIc), CA1873 (VGIIIa) and CA1508 (VGIIIb). Fluorescence intensity values for
1131 untreated, isotype control and Crp127-treated cells are presented in red, blue and
1132 orange, respectively, with corresponding MFI values displayed in the top left, centre
1133 and right of each panel. *C. gattii* strains **C)** DSX, **E)** R265, **F)** CDCR272, **G)** CA1873
1134 and **H)** CA1508 were labelled for chitin (blue; CFW) and Crp127 (far-red; goat Alexa-
1135 647-conjugated anti-mouse IgM μ -chain) and maximum-intensity projections
1136 generated via confocal microscopy. Presented are representative images merged for
1137 transmitted light and Crp127 (left panels) and Crp127 and chitin (right panels). Scale
1138 bars represent $5 \mu\text{m}$.

1139

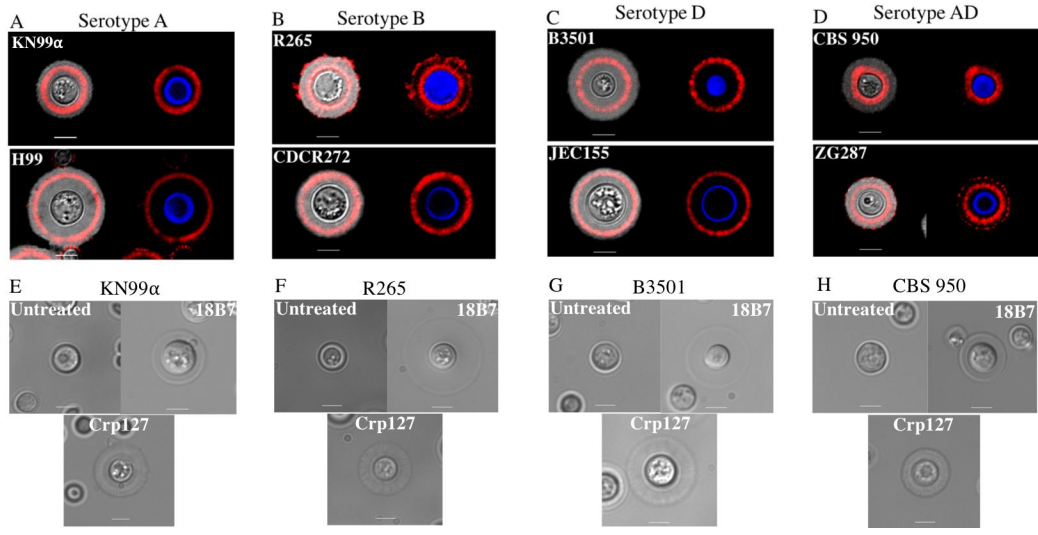
1140

1141

1142

1143

1144



1145

1146

1147

1148

1149

1150

1151

1152

1153

1154

1155

1156

1157

1158

1159

1160

1161 **Fig. 6. The Crp127 epitope is spatially confined to distinct capsular regions**
1162 **and binding elicits capsular swelling reactions distinct from those of 18B7.**
1163 *Cryptococcus* cells were grown in capsule-inducing conditions and imaged to
1164 determine the location of the Crp127 epitope within the enlarged capsule and
1165 characterise the capsular reaction patterns elicited by this antibody. *Cryptococcus*
1166 strains from **A)** serotype A (KN99 α and H99), **B)** serotype B (R265 and CDCR272,
1167 **C)** serotype D (B3501 and JEC155) and **D)** serotype AD (CBS 950 and ZG287) were
1168 labelled for chitin (blue; CFW) and Crp127 (far-red; goat Alexa-647-conjugated anti-
1169 mouse IgM μ -chain), suspended in Indian ink to visualise the capsule and imaged
1170 using confocal microscopy. Representative images of a single focal plane are shown
1171 for each strain. Presented are images merged for transmitted light and Crp127 (left
1172 panels) and Crp127 and chitin (right panels). Capsule-induced cells of strains **E)**
1173 KN99 α , **F)** R265, **G)** B3501 and **H)** CBS 950 were also left untreated (top right
1174 panels), treated with mAb 18B7 (top right panels) or with mAb Crp127 (bottom
1175 panels) and imaged using DIC microscopy to observe capsular reaction patterns.
1176 Scale bars represent 5 μ m.

1177

1178

1179

1180

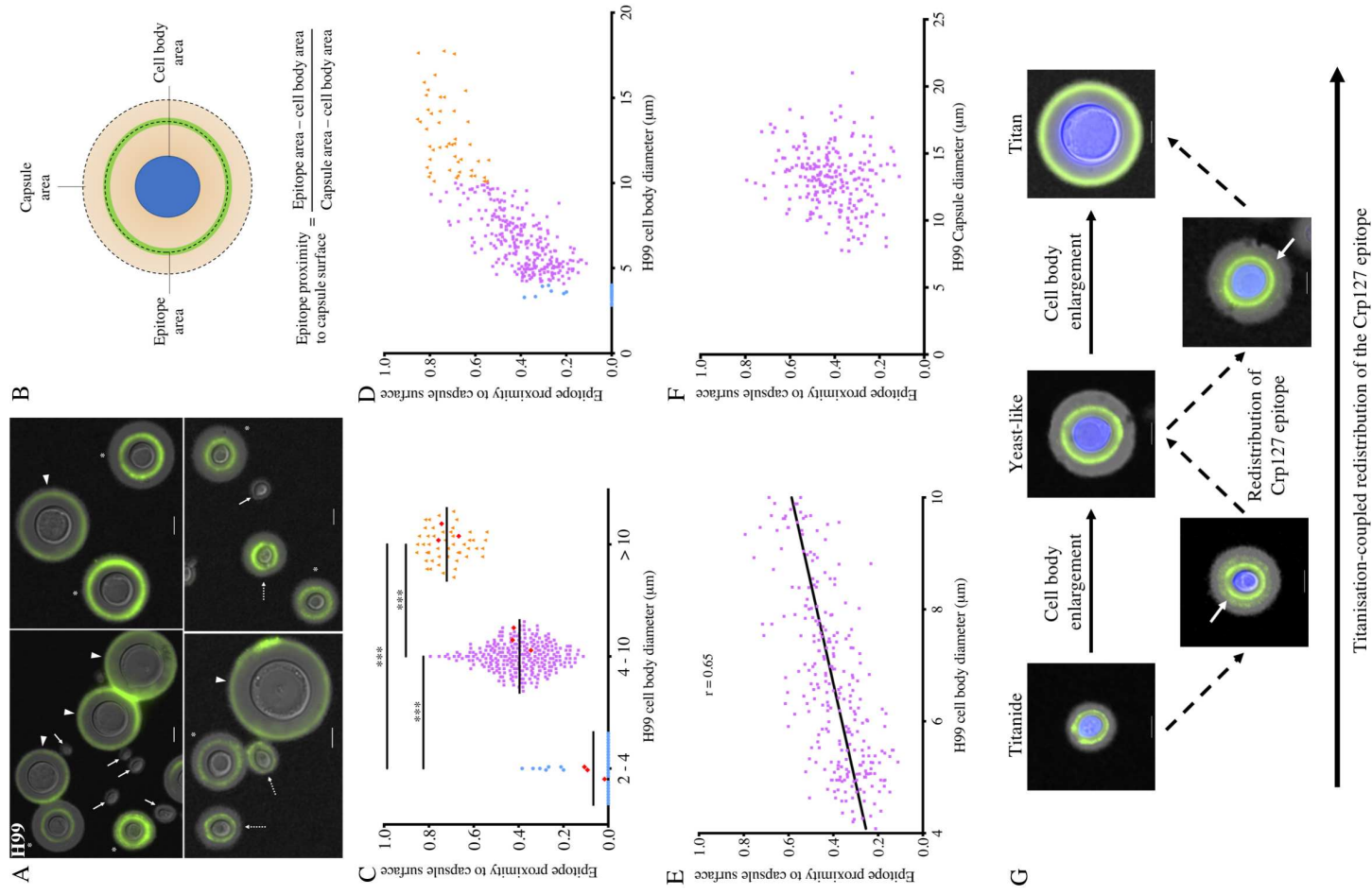
1181

1182

1183

1184

1185

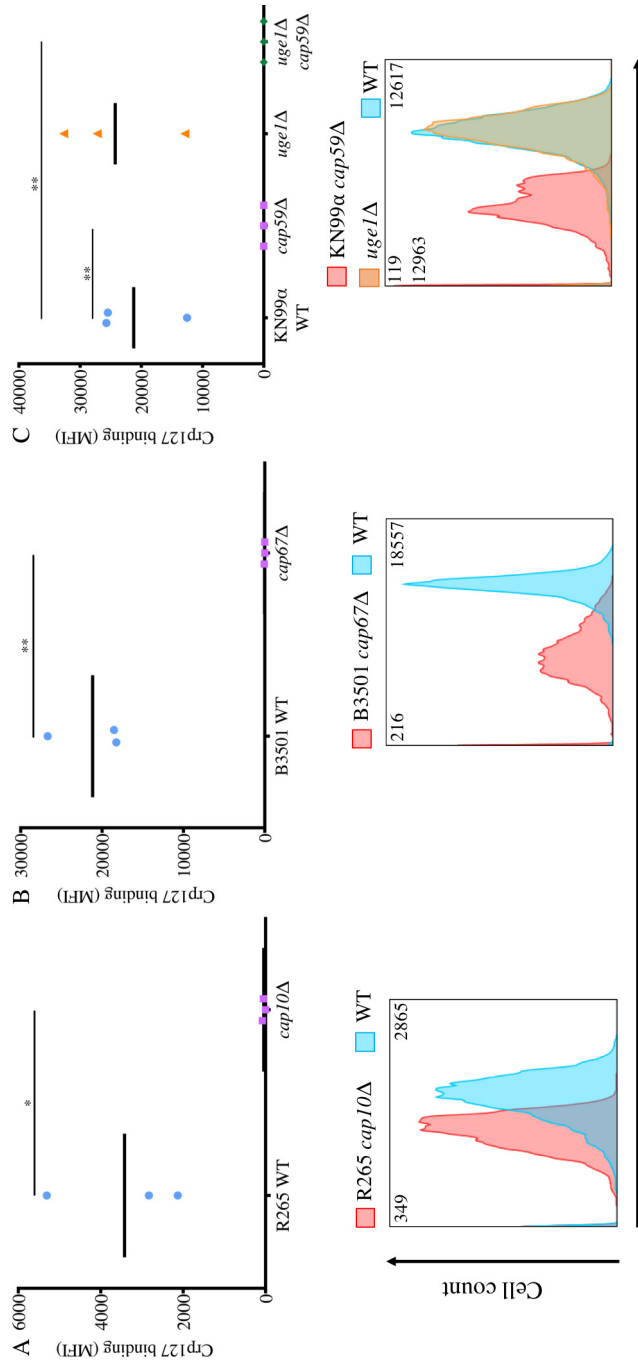


1186

1187

1188 **Fig. 7. Spatial distribution of the Crp127 epitope differs within the capsule of**
1189 **the three cell subtypes found in Titanising populations of strain H99,**
1190 **suggesting a model of Titanisation-coupled epitope redistribution.** Cultures of
1191 *C. neoformans* strain H99 that derived solely from Titan cells were investigated for
1192 differences in the capsular distribution of the Crp127 epitope. **A)** Representative
1193 images of cells from strain H99 grown under conditions permissive for Titanisation,
1194 resulting in formation of Titanide (block arrows and dashed arrows distinguish no
1195 Crp127 binding and binding, respectively), yeast-like (asterisks) and Titan cells
1196 (arrowheads). **B)** A schematic representation of how Crp127 epitope proximity to the
1197 capsule surface was quantified through the analysis of micrographs using ImageJ.
1198 Where no antibody binding was detected, the ratio was calculated as 0. **C)** The
1199 proximity of the Crp127 epitope to the capsule surface of 2-4 μm , 4-10 μm and >10
1200 μm cells of strain H99 was quantified. Data points represent all individual cells for
1201 which the location of the Crp127 epitope was quantified, whilst the horizontal bar
1202 represents the mean of pooled cells. Red diamonds represent mean values
1203 calculated from each of three biological repeats. Tukey's multiple comparisons test
1204 was used to test for statistically significant differences between the three groups
1205 ($n=3$) (** $P < 0.01$; *** $P < 0.001$). **D)** Cell body diameter was plotted against the
1206 epitope proximity to the capsule surface for all cells measured and from **E)** cells 4-10
1207 μm in cell body diameter. **F)** Capsule diameter was plotted against the epitope
1208 proximity to the capsule surface for cells 4-10 μm in cell body diameter. **G)** Model
1209 for Titanisation-coupled redistribution of the Crp127 epitope. Presented are
1210 representative images of Titanide, yeast-like and Titan cells (top row) of strain H99
1211 that were recognised by Crp127, in addition to Titanide and yeast-like cells exhibiting

1212 a second faint ring of antibody binding (white arrows) (bottom row). Scale bars
1213 represent 5 μm .



Crp127 binding

